Analysis of Loudspeaker Line Arrays*

MARK S. UREDA, *AES Member*

JBL Professional, Northridge, CA 91329, USA

A set of mathematical expressions to analyze the performance of loudspeaker line arrays is provided. At first a set of expressions for straight-line arrays is developed, including the directivity function, polar response, quarter-power angle, on-axis and off-axis pressure responses, and two-dimensional pressure field. Since in practice many loudspeaker line arrays are not actually straight, expressions are provided for curved (arc), J, and progressive line arrays. In addition, since loudspeaker systems are often not perfect sources, the effects of spherical radiating sources and gaps between sources are analyzed. Several examples of how to apply the models are given, and modeled performance is compared to measured polar data.

0 INTRODUCTION

Vertical line arrays of loudspeakers are at present gaining prominence among sound-reinforcement professionals. That is not to say that they are an entirely new concept. Indeed, Klepper and Steele wrote in 1963 [1]: "Line-source loudspeaker arrays, often called 'column' loudspeakers, have recently become of great interest to sound-system contractors and equipment manufacturers in this country."

What *is* new is that loudspeaker manufacturers have applied good engineering practice to long known principles of line source physics. Systems today provide well-behaved directivity response, high output power, and high-quality sound over an extended frequency range. Together these represent a significant improvement in performance over conventional column loudspeakers.

Column loudspeakers typically comprise a vertical stack of full-range direct radiators. They produce modest sound power levels and exhibit a vertical directivity response that changes substantially with frequency. Klepper and Steele describe problems with column loudspeakers, including "narrowing of the major (on-axis) lobe at higher frequencies" and "strong minor off-axis lobes or sidelobes at high frequencies." These, they write, are predicted by equations given by Olson [2]. Their paper prescribes methods for improving the polar response, but the success of these techniques is limited by the directional characteristics of the individual loudspeakers themselves, which narrow at high frequency.

Today manufacturers of loudspeaker line arrays often provide specially designed waveguides in place of individual direct radiators for the high-frequency band. This is an important improvement. While column loudspeakers behave like an array of individual, frequency-dependent acoustic sources, contemporary systems behave more like continuous line sources. This allows them to achieve a well-behaved directivity response to very high frequency.

Manufacturers have also realized that long, perfectly straight loudspeaker line arrays produce a directivity response that often becomes too narrow at high frequencies for many sound-reinforcement venues. In fact, they have learned that it is often desirable to produce an asymmetrical response in the vertical plane, for instance, one that projects energy forward and downward at the same time. This can be achieved if the array is slightly curved, particularly along the lower portion. Recently manufacturers have designed line array loudspeaker systems that can be curved over the entire length of the array while maintaining the attributes of a continuous source. This allows users to achieve simultaneously the narrow, long throw characteristics of a straight-line array and the wide, lower fill characteristics of a curved array.

This paper provides mathematical expressions for estimating the performance of a wide variety of line arrays. The models are based on theoretical line sources, but the estimates obtained agree quite well with measurements taken on real-life line arrays, particularly those from the latest generation of loudspeaker systems designed specifically for line array applications.

1 BACKGROUND AND OVERVIEW

Most analyses of line sources reference Wolff and Malter's [3] seminal work of 1930. Wolff and Malter develop expressions for the polar response of a linear array of point

*Manuscript received 2003 July 24; revised 2004 February 23.

sources in the far field. The far-field restriction allows the directivity function to be expressed in closed form. Their paper has been referenced and/or augmented over the years by Beranek [4],[1] Wood [5], Davis [6], Rossi [7], and Skudrzyk [8] among others. For the convenience of the reader, Sections 2.1 through 2.4 summarize important elements of their work as well.

Section 2.5 analyzes the on-axis pressure response of line sources. Here the far-field restriction is abandoned, and the pressure is expressed as a function of distance. This analysis follows the work of Lipshitz and Vanderkooy [9] and Smith [10], who present the on-axis and off-axis pressure responses of line sources. They show that the pressure response undulates near the source while generally decreasing in level at −3 dB per doubling of distance. At a certain distance, referred to as the transition distance,[2] the undulations disappear and the response falls off at −6 dB. The near field is defined as the region between the source and the transition distance. Beyond the transition distance is the far field. The transition distance is a function of the line source length and frequency and has been estimated by Smith [10], Heil [12],[3] Junger and Feit [13], and Ureda [14, p. 6].

The pressure response of a line source on either side of the transition distance, however, is more complex than the on-axis pressure response would suggest. In fact, depending on the point chosen along the source from which one begins the pressure response analysis, different results are obtained. Section 2.5 explores this complexity by comparing the results obtained when different points along a straight-line source are taken as the initial point. It is shown that each of these responses represents different slices through the pressure field. The mathematical expression for the pressure field of a straight-line source is given in Section 2.6.

As illustrated throughout Section 2, straight-line sources produce polar response curves that vary substantially with length and frequency. At long lengths and high frequencies they get very narrow, often too narrow for sound-reinforcement venues. Curved or arc sources, however, produce polar response curves that are materially wider and approach the included angle of the arc at high frequency. This has been described in many of the texts cited earlier, including Wolff and Malter [3],[4] Olson [2],[5] and Rossi [7, p. 134]. Section 3 of this paper expands on the analysis of arc sources by providing mathematical expressions for the polar response, on-axis pressure response, and two-dimensional pressure field.

Arc sources, while useful by themselves in certain sound-reinforcement venues, are of particular interest when used in conjunction with straight-line sources. The combination is referred to as a J source [15]. J sources are comprised of a straight-line source placed above and adjacent to an arc source. The straight segment provides long throw and the arc segment provides coverage in the down front region. Together they provide an asymmetrical polar response in the vertical plane that is well suited for many venues. Section 4 describes J sources and provides expressions for the polar response, on-axis response, and two-dimensional pressure field.

Like a J source, a progressive[6] source [15] also provides an asymmetrical polar response in the vertical plane. Unlike a J source, however, a progressive source is a continuous curve. The upper portion of the source is nearly straight but then increases in curvature toward the bottom. Section 5 provides expressions for its polar response, on-axis pressure response, and two-dimensional pressure field. These show that a progressive source produces a response that is remarkably constant with frequency.

In practice, even with specially designed loudspeaker systems, large line arrays are not perfectly continuous line sources. They invariably have gaps between the individual array elements, which are essentially nonradiating portions of the total line source. Certain effects of such discontinuities are described by Urban et al. [16]. Section 6 expands on this work and analyzes the polar responses of straight-line sources with various size gaps. It provides guidelines for acceptable gap-to-wavelength ratios.

Urban et al. also describe certain effects produced if the radiating elements in loudspeaker line arrays produce radial wavefronts instead of pure, flat wavefronts. He models this as a stack of slightly curved sources. Section 6 examines the polar response of this stack and shows that grating lobes occur at high frequency or large curvature.

Finally, it is important to examine how closely the mathematical models developed in this paper estimate the performance of loudspeaker line arrays. Section 7 compares the modeled and measured polar response curves of three loudspeaker line arrays. Despite the vagaries of real-life sources and measurement challenges, the models provide remarkably good estimates of array performance over a wide frequency range. Button [17] and Engebretson et al. [18] compare measured results against predictions produced by models similar to the ones developed in the present paper. Section 7 takes measured results from Engebretson et al. and compares them directly against predictions produced explicitly by the straight-line source and arc source models developed in the following sections.

[1]The author shows the polar response (in dB) of line sources (p. 96) and curved sources (p. 106).

[2]"Transition" distance is used instead of "critical" distance to avoid confusion with the term "critical distance" used in architectural acoustics, where it refers to the distance at which the direct and reverberant fields are equal in level. See Eargle [11].

[3]The author discusses the response of line arrays in the near field (Fresnel region) and the far field (Fraunhofer region).

[4]See page 212 for a discussion on curved line sources.

[5]See p. 27, where Olson provides the directional characteristics of 60, 90, and 120° arc sources.

[6]The term "progressive" is used in the present paper instead of "spiral" originally used by the author. The term spiral array is sometimes used in reference to so-called barber-pole arrays, as in Klepper and Steele [1].

2 STRAIGHT-LINE SOURCES

2.1 Directivity Function of Straight-Line Sources—General Form

A line source can be modeled as a continuum of infinitely small line segments distributed along a line. The acoustic pressure radiated from a line source[7] is

$$p = \int_{-L/2}^{L/2} \frac{A(l)\mathrm{e}^{-\mathrm{j}[kr(l)+\varphi(l)]}}{r(l)}\,\mathrm{d}l$$

where L is the length of the line source, $A(l)$ is the amplitude function along the line, $\varphi(l)$ is the phase function along the line, k is the wavenumber, and $r(l)$ is the distance from any segment $\mathrm{d}l$ along the line to the point of observation ***P***.

The evaluation of this expression is simplified if we assume that the observation point ***P*** is a large distance away, that is, the distance is much greater than the length of the source, and the distances to ***P*** from any two segments along the line are approximately equal. This allows us to bring the $r(l)$ term in the denominator to the front of the integral since, by definition,

$$\frac{1}{r(L/2)} \approx \frac{1}{r(-L/2)} \approx \frac{1}{r}.$$

Conversely, the $r(l)$ term in the exponential has a significant influence on the directivity function. This is because the relatively small distance differences to ***P*** from any two segments are not small compared to a wavelength, particularly at high frequency. Fig. 1 shows that $r(l)$ in the exponent can be expressed as

$$r(l) = l \sin \alpha$$

where α is the angle between a line bisecting the source and a line from the midpoint of the source to ***P***. Substituting, the far-field pressure at angle α of a line source is

$$p(\alpha) = \frac{1}{r}\int_{-L/2}^{L/2} A(l)\ \mathrm{e}^{-\mathrm{j}[kl \sin \alpha+\varphi(l)]}\,\mathrm{d}l.$$

[7]The time-varying factor $\mathrm{e}^{\mathrm{j}\omega t}$ is omitted.

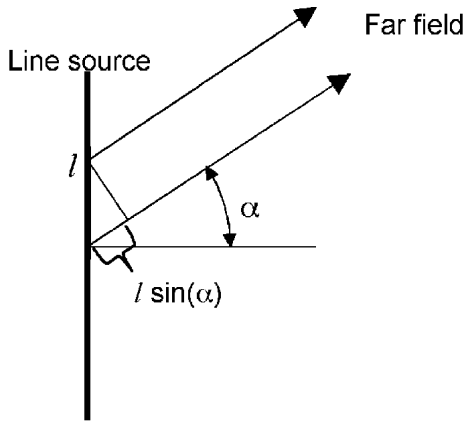

Fig. 1. Geometric construction for far-field directivity function of a line source.

The directivity function $R(\alpha)$ of a line source is the magnitude of the pressure at angle α over the magnitude of the maximum pressure that can be obtained, that is,

$$R(\alpha) = \frac{|p(\alpha)|}{|p_{\max}|}.$$

The maximum radiated pressure is obtained when all segments along the line radiate in phase, that is, the exponential function equals unity.[8] It is given as

$$p_{\max} = \frac{1}{r}\int_{-L/2}^{L/2} A(l)\,\mathrm{d}l.$$

The general form of the far-field directivity function $R(\alpha)$ of a line source is then

$$R(\alpha) = \frac{\left|\int_{-L/2}^{L/2} A(l)\ \mathrm{e}^{-\mathrm{j}[kl \sin \alpha+\phi(l)]}\,\mathrm{d}l\right|}{\left|\int_{-L/2}^{L/2} A(l)\,\mathrm{d}l\right|}.$$

2.2 Directivity Function of Straight-Line Sources—Uniform Amplitude and Phase

The general form of the straight-line source directivity function developed in Section 2.1 is valid for any amplitude and phase functions along the length of the line source. A uniform line source has constant amplitude and zero phase shift along its length, that is, $A(l) = A$ and $\phi(l) = 0$. Substituting into the general form yields an expression for the directivity function of a uniform line source $R_{\mathrm{U}}(\alpha)$,

$$R_{\mathrm{U}}(\alpha) = \frac{1}{L}\left|\int_{-L/2}^{L/2} \mathrm{e}^{-\mathrm{j}kl \sin \alpha}\,\mathrm{d}l\right|.$$

Solving the integral and applying Euler's identities, this becomes

$$R_{\mathrm{U}}(\alpha) = \frac{\sin\left[(kL/2)\sin\alpha\right]}{(kL/2)\sin\alpha}$$

or in terms of wavelength instead of frequency,

$$R_{\mathrm{U}}(\alpha) = \frac{\sin\left[(\pi L/\lambda)\sin\alpha\right]}{(\pi L/\lambda)\sin\alpha}.$$

Fig. 2 shows polar response curves[9] of a uniform line source at various ratios of source length and wavelength. The polar response is wide at low ratios of L/λ. As the ratio is increased, the directivity pattern narrows and exhibits nulls and lobes. These are explored in more detail in Section 2.3.

[8]Note that the maximum pressure at any given distance and frequency may never actually be obtained.

[9]A polar response curve is the directivity function expressed in decibels and plotted on a polar chart. The on-axis pressure is used as the reference pressure, that is, polar response $= 20 \log [R(\alpha)/R(0)]$.

2.3 Lobes and Nulls—Uniform Straight-Line Source

Fig. 2 shows that at long wavelengths ($\lambda > L$) the polar response of a uniform straight-line source is fairly omnidirectional. At shorter wavelengths lobes and nulls are obtained. The position and magnitude of these are easily calculated.

The far-field directivity function of a uniform line source is given in Section 2.2 as

$$R_U(\alpha) = \frac{\sin\left[(\pi L/\lambda)\sin\alpha\right]}{(\pi L/\lambda)\sin\alpha}.$$

This function has the generic form of sin z/z. To evaluate this function on axis, that is, $z = 0$, we must use L'Hospital's rule, taking derivatives of the numerator and denominator. This yields

$$\lim \frac{\sin z}{z} \rightarrow \cos(0) = 1.$$

The fact that the limit approaches unity indicates that there will always be a maximum on axis. Off-axis nulls are obtained when sin z/z goes to zero. This occurs where the argument z reaches (nonzero) multiples of π. Substituting the full expression for z, nulls are obtained when

$$\frac{\pi L}{\lambda}\sin\alpha = m\pi$$

where m is a nonzero integer. Therefore nulls are obtained at

$$|\sin\alpha| = m\frac{\lambda}{L}$$

where $m = 1, 2, 3, \ldots$. Off-axis lobes of the directivity function are found between the nulls, that is, at

$$|\sin\alpha| = \frac{3\lambda}{2L}, \frac{5\lambda}{2L}, \frac{7\lambda}{2L}, \ldots.$$

This can be written as

$$|\sin\alpha| = \frac{(m + 1/2)\lambda}{L}$$

where $m = 1, 2, 3, \ldots$.

Finally it is possible to calculate the amplitude of the lobes of a uniform line source. Since the amplitude decreases inversely with z, the pressure amplitude of the mth lobe is

$$A_m = \left|\frac{\cos(m\pi)}{m\pi + \pi/2}\right|$$

where $m = 1, 2, 3, \ldots$.

2.4 Quarter-Power Angle—Uniform Straight-Line Source

Often it is useful to determine the −6-dB angle of a uniform straight-line source. This is accomplished by setting the generic form of the directivity function equal to 0.5,[10] that is,

$$\frac{\sin z}{z} = 0.5.$$

[10]The directivity function is a pressure ratio. A pressure ratio of 0.5 yields a sound pressure level difference of −6 dB.

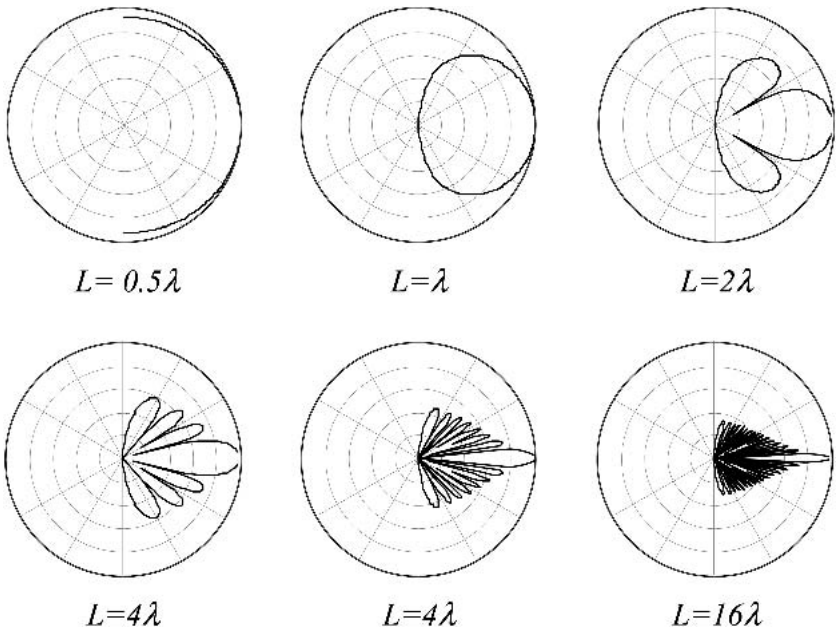

Fig. 2. Polar response curves of a uniform line source.

Solving numerically, $z = 1.895$. The −6-dB point on one side of the central lobe is at angle α, where

$$z = 1.895 = \frac{\pi L}{\lambda} \sin \alpha.$$

The quarter-power angle is the total included angle between the −6-dB points on either side of the central lobe and is given by

$$\theta_{-6\,\mathrm{dB}} = 2\alpha.$$

Solving for α in terms of length and wavelength and substituting we have

$$\theta_{-6\,\mathrm{dB}} = 2 \sin^{-1} \frac{1.895\lambda}{\pi L}$$

$$\approx 2 \sin^{-1} \frac{0.6\lambda}{L}.$$

The quarter-power angle as a function of L/λ is shown in Fig. 3. A similar result is obtained by Benson [19].[11]

At small L/λ, that is, a short line source and long wavelength, the quarter-power angle is wide. At large ratios of L/λ, that is, long sources and short wavelengths, the quarter-power angle is narrow. For small angles,[12] where $\sin z \approx z$, the line source quarter-power angle is

$$\theta_{-6\,\mathrm{dB}} = \frac{1.2\lambda}{L}$$

where θ is in radians. Expression θ in degrees, we have

$$\theta_{-6\,\mathrm{dB}} = 68.8 \frac{\lambda}{L} \qquad \text{(degrees)}.$$

[11]Note that Benson solved for the −3-dB angle.

[12]The small angle approximation holds for angles less than about 30°. Note that $\sin(\pi/6) = 0.5000$ and $\pi/6 = 0.5235$ so that the error is less than 5%.

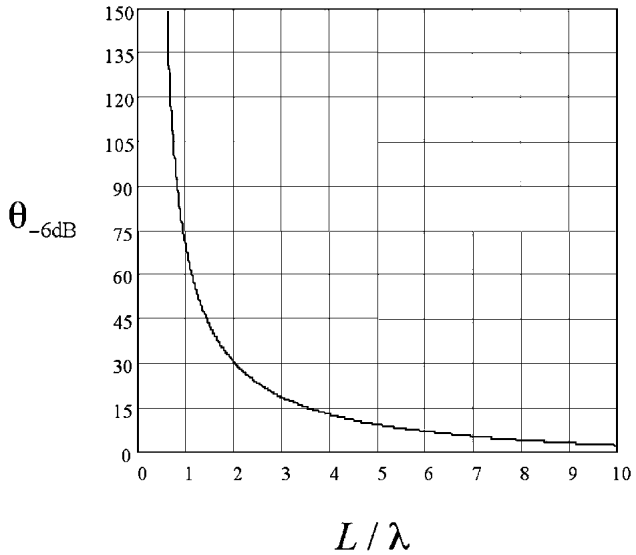

Fig. 3. Quarter-power angle of a uniform line source.

In some cases it is convenient to use frequency rather than a ratio of wavelength and source length. Rewriting, the quarter-power angle equation for uniform line sources becomes (approximately)

$$\theta_{-6\,\mathrm{dB}} \approx \frac{2.4 \times 10^4}{fL}$$

for L in meters and f in hertz, or

$$\theta_{-6\,\mathrm{dB}} \approx \frac{7.8 \times 10^4}{fL}$$

for L in feet and f in hertz.

The directivity response of a line source is a plot of the quarter-power angle versus frequency. The directivity response of uniform line sources of several lengths is shown in Fig. 4. These show that the quarter-power angle of large sources is quite narrow at high frequency. For instance, at 10 kHz a 4-m-long uniform straight-line source has a −6-dB angle of 0.6°.

2.5 On-Axis Pressure Response of Straight-Line Sources

The on-axis pressure response of a line source is derived in much the same manner as the directivity function. The pressure radiated from each infinitely small line segment is summed at an observation point ***P.*** In this case, however, ***P*** is at a distance x along an axis normal to the source and no far-field assumptions are made.

2.5.1 Conventional Approach—Midpoint Method

Fig. 5 shows the conventional geometric construction used to solve for the pressure along a path normal to the source, beginning at its midpoint. Referring to Fig. 5, L is

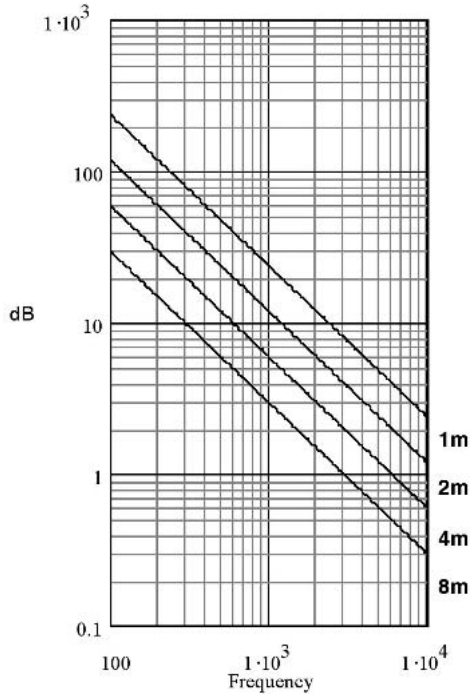

Fig. 4. Directivity response of uniform line sources 1, 2, 4, and 8 m long.

the total length of the source and r_{mid} is the distance from any radiating element dl of the source to any distance x along the horizontal axis. The general form for the radiated pressure at x is

$$p_{mid}(x) = \int_{-L/2}^{L/2} \frac{A(l)\, e^{-j[kr_{mid}(x,\, l)+\varphi(l)]}}{r_{mid}(x,\, l)}\, dl$$

where

$$r_{mid}(x,\, l) = \sqrt{x^2 + l^2}\,.$$

The pressure response is the logarithmic ratio of the magnitude of the pressure squared at x over the magnitude of the pressure squared at some reference distance, that is,

$$R(x) = 20 \log \frac{|p(x)|}{|p(x_{ref})|}\,.$$

The on-axis pressure response of a 4-m uniform straight-line source, where $A(l) = A$ and $\varphi(l) = 0$, at 8 kHz is shown in Fig. 6. The pressure response generally decreases at a rate of −3 dB per doubling of the distance out to approximately 100 m. It exhibits undulations in this region, the magnitudes of which increase as the distance approaches 100 m. Beyond 100 m the pressure amplitude no longer undulates and decreases monotonically at −6 dB per doubling of the distance. The point at which this change occurs is referred to as the transition distance. The region between the source and the transition distance is referred to as the near field, and the region beyond is the far field.

The transition distance varies with source length and frequency. Fig. 7 shows the on-axis response of three different-length uniform line sources at 8 kHz. As the length L increases, the transition distance increases. Fig. 8 shows the on-axis response of a 4-m-long uniform line source at 500 Hz, 2 kHz, and 8 kHz. It illustrates that the transition distance also increases with frequency.

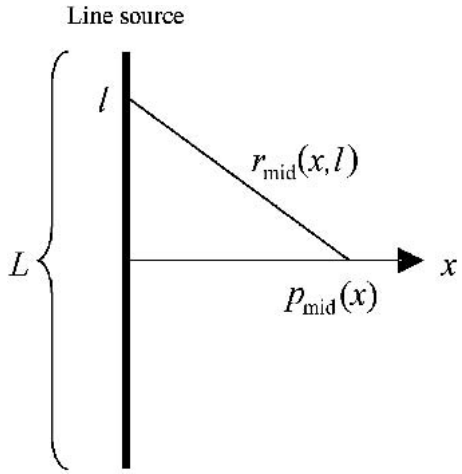

Fig. 5. Geometric construction for calculating on-axis pressure response of a line source (midpoint convention).

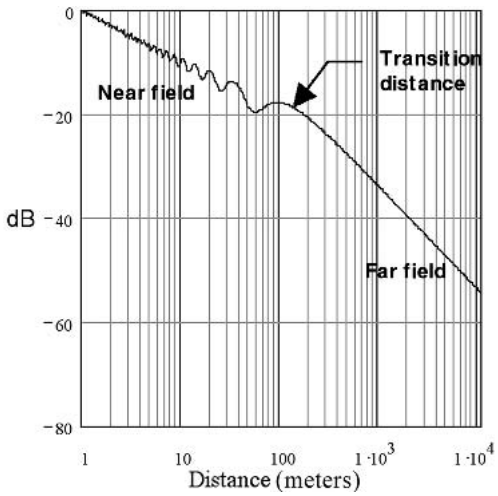

Fig. 6. On-axis pressure response (from midpoint) of a uniform line source (4 m long, 8 kHz).

2.5.2 Midpoint versus Endpoint

The conventional approach used to determine the on-axis pressure response of a line source discussed in Sec-

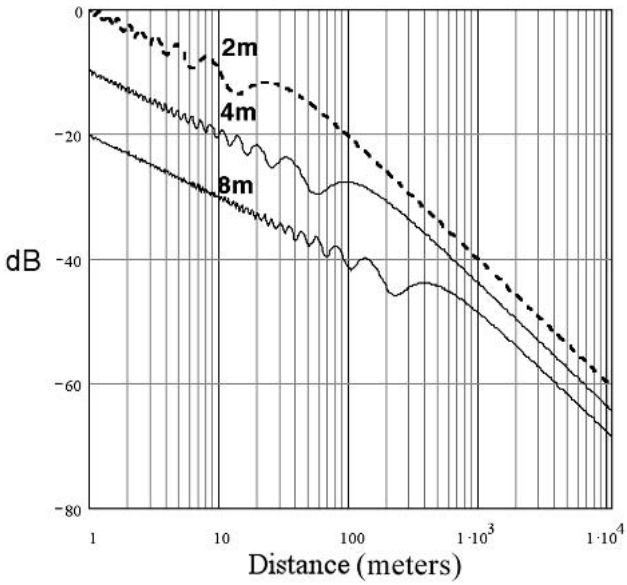

Fig. 7. On-axis response (from midpoint) of 2; 4; and 8-m uniform line sources at 8 kHz. 4- and 8-meter response curves are offset by 10 and 20 dB, respectively.

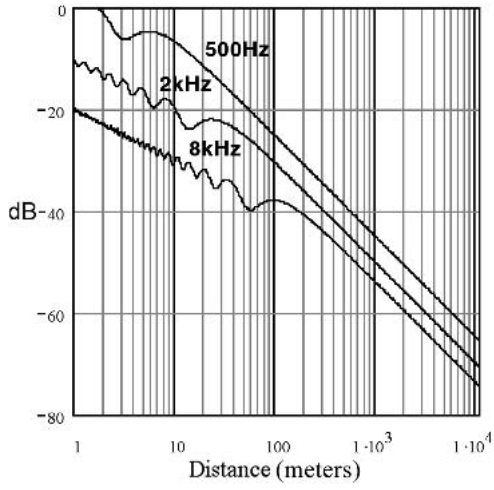

Fig. 8. On-axis response (from midpoint) of a 4-m uniform line source at 500 Hz, 2 kHz, and 8 kHz. 2- and 8-kHz response curves are offset by 10 and 20 dB, respectively.

tion 2.5.1 is to take a path normal to the source beginning at its midpoint. This yields a result, however, that is unique to this path. Choosing the midpoint as the initial point introduces symmetry into the analysis and minimizes the apparent aperture of the source. If a different initial point is chosen, the line source appears longer on one side of this point than on the other side. This difference is maximized when the endpoint of the source is chosen. In this case the source has length L in one direction and zero length in the other. If the on-axis pressure is summed along a path normal to the source beginning at the endpoint of the line source, the transition distance increases substantially.

Fig. 9 shows a modified geometric construction for calculating the on-axis pressure response. The pressure summed along a path normal to the endpoint of a line source is

$$p_{\text{end}}(x) = \int_{-L/2}^{L/2} \frac{A(l)\, \mathrm{e}^{-\mathrm{j}[kr_{\text{end}}(x,\, l)+\varphi(l)]}}{r_{\text{end}}(x,\, l)}\, \mathrm{d}l$$

where

$$r_{\text{end}}(x,\, l) = \sqrt{x^2 + \left(l + \frac{L}{2}\right)^2}.$$

Fig. 10 compares the on-axis response of a 4-m-long uniform straight-line source, where $A(l) = A$ and $\varphi(l) = 0$, at 8 kHz using the midpoint and endpoint methods. The last peak of the midpoint near-field response occurs at approximately 100 m. The last peak of the endpoint response occurs at approximately 400 m. Note that the endpoint response is at a lower amplitude level than the midpoint response in the near field. In the far field the curves converge and yield the monotonic decrease of −6 dB per doubling of the distance as described.

If the origin of the path is moved beyond the endpoint, the distance to the last peak occurs at greater and greater distances. It can be shown that the distance to the far field continues to increase as one chooses a path further off the midpoint axis. However, the pressure levels fall off quite dramatically once the endpoint is breeched. This is shown in Fig. 11. The first two curves labeled "0" and "L/2" are the midpoint and endpoint pressure responses, respectively, shown in Fig. 10. The next two curves are on-axis pressure response curves beginning at points one length (L) and three half-lengths (3L/2) displaced vertically from the midpoint.

The curves in Fig. 11 are slices through the pressure field, normal to the source, at increasing displacement from the midpoint. We can see that as the origin of the path is moved off the midpoint, the amplitude levels of the pressure decreases in the near field. It is approximately −6 dB at the endpoint, but decreases to around −40 dB at L and 3L/2. Also, the pressure response curves L and 3L/2 undulate in a fashion that in the aggregate is nearly flat from the source to the far field.

The L and 3L/2 response curves are so low in level relative to the midpoint response that they are of limited significance. However, the endpoint curve (L/2) is a material feature of the pressure field. It is approximately −6 dB down from the midpoint response and undulates

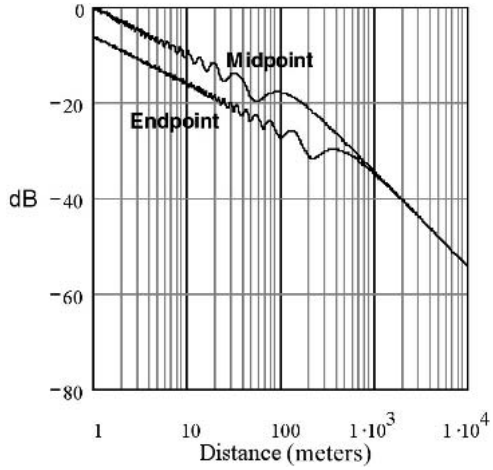

Fig. 10. Comparison of midpoint and endpoint pressure response curves of a 4-m uniform line source at 8 kHz.

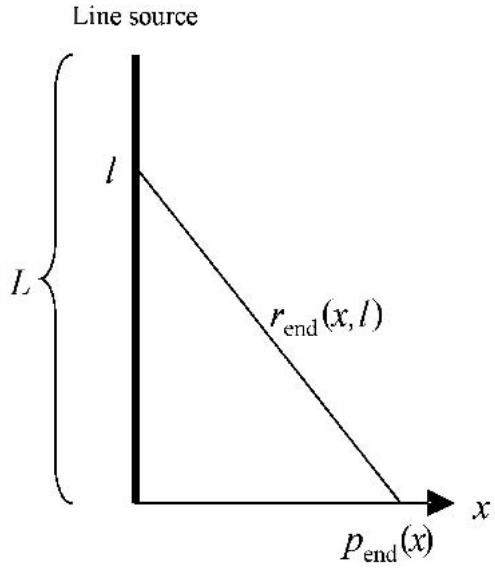

Fig. 9. Geometric construction for calculating pressure response along a path originating at the endpoint.

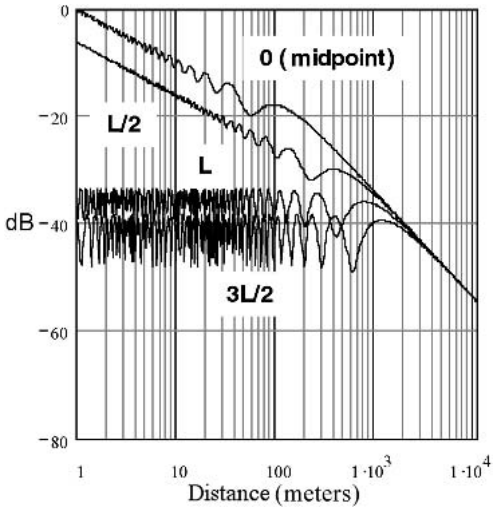

Fig. 11. Pressure response along paths normal to line source at various points of origin (4 m at 8 kHz).

well past the midpoint transition distance. The fact that two such disparate response curves can be obtained by merely shifting the origin of the normal path demonstrates the ambiguity of the term "on-axis response."

2.6 Pressure Field of Straight-Line Sources

The most comprehensive approach to observe the pressure response of a line source is to compute its pressure field. This eliminates the question of midpoint versus endpoint. It is obtained by rewriting the expression for the radiated pressure in terms of Cartesian coordinates as set up in Fig. 12. The pressure at any point $\boldsymbol{P}$ is

$$p(x, y) = \int_{-L/2}^{L/2} \frac{A(l)\, e^{-j[kr(x, y, l)+\varphi(l)]}}{r(x, y, l)}\, dl$$

where

$$r(x, y, l) = \sqrt{x^2 + (y - l)^2}.$$

Fig. 13 shows the pressure field of a 4-m uniform straight-line source, where $A(l) = A$ and $\varphi(l) = 0$, in several frequency bands. The major on-axis lobe gets narrower with increasing frequency, as expected. The minor lobes increase in number and lower amplitude levels. At high frequency they dissolve into very complex patterns of constructive and destructive interference. Note that the pressure varies across the major lobe at 8 kHz in a manner consistent with the pressure slices shown in Fig. 11. The undulations extend to a greater distance from a line normal to the endpoint than from the midpoint.

3 ARC SOURCES

Many loudspeaker line arrays used in practice are actually curved. This is because pure straight-line arrays produce a narrow vertical polar response at high frequency—often too narrow to reach audiences beneath and slightly in front of the array. A slightly curved array provides superior coverage in this area. One important type of curved line source is the arc source.

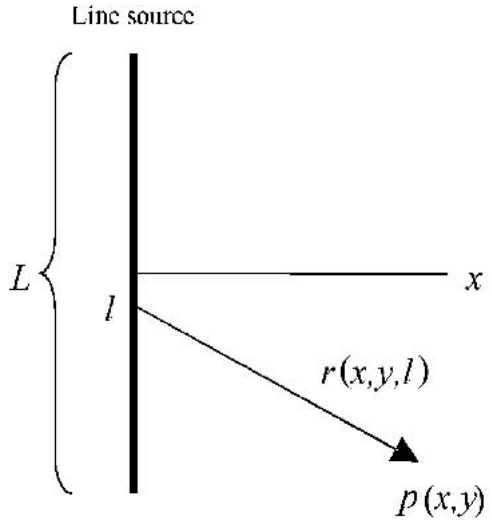

Fig. 12. Geometric construction for pressure field of a line source.

An arc source is comprised of radiating elements arranged along a segment of a circle. At all frequencies it provides a wider directivity response than a straight-line source of the same length. At high frequency it provides a polar pattern that corresponds to the included angle of the arc.

3.1 Polar Response of Arc Sources

The derivation of the directivity function of an arc source follows the same steps as described for a straight-line source. Fig. 14 shows the geometric construction of an arc source with radius $\boldsymbol{R}$ and total included angle θ. The pressure radiated by an arc at off-axis angle α is

$$p_A(\alpha) = \int_{-\theta/2}^{\theta/2} \frac{A(\phi)\, e^{-j[kr_A(\phi, \alpha)+\varphi(\phi)]}}{r_A(\alpha, \phi)}\, \boldsymbol{R}\, d\phi.$$

As in Section 2.1, the evaluation of this expression is simplified if we assume that the observation point $\boldsymbol{P}$ is a large distance away. In this case the distance is much greater than the length of the arc, and the distances to $\boldsymbol{P}$ from any two segments along the arc are approximately equal. This allows us to bring the r_A term in the denominator to the front of the integral since by definition

$$\frac{1}{r_A(\theta/2)} \approx \frac{1}{r_A(-\theta/2)} \approx \frac{1}{r_A}.$$

Conversely, the r_A term in the exponential has a significant influence on the directivity function. This is because the relatively small differences in distance to $\boldsymbol{P}$ from any two segments are not small compared to a wavelength. Fig. 14 shows that r_A in the exponent can be expressed as

$$r_A(\alpha, \phi) = 2\boldsymbol{R} \sin\left(\frac{\phi}{2}\right) \sin\left(\frac{\phi}{2} + \alpha\right)$$

where α is the angle between a line that bisects the arc angle and a line from the center point of the arc to $\boldsymbol{P}$. Substituting, the far-field directivity function of an arc is then expressed in general form as

$$R_A(\alpha) = \left| \frac{\int_{-\theta/2}^{\theta/2} A(\phi)\, e^{-j[kr_A(\alpha, \phi)+\varphi(\phi)]} \boldsymbol{R}\, d\phi}{\int_{-\theta/2}^{\theta/2} A(\phi) \boldsymbol{R}\, d\phi} \right|.$$

If we assume constant amplitude and zero phase shift along the arc, that is, $A(\phi) = A$ and $\varphi(\phi) = 0$, the directivity function reduces to[13]

$$R_A(\alpha) = \frac{1}{\boldsymbol{R}\theta} \left| \int_{-\theta/2}^{\theta/2} e^{-jkr_A(\alpha, \phi)} \boldsymbol{R}\, d\phi \right|$$

[13]This integral does not have a convenient closed-form solution similar to the one obtained for the line array. Wolff and Malter [3] provide a point source summation version of the directivity function as follows:

$$R(\alpha) = \frac{1}{2m + 1} \left| \sum_{n=-m}^{n=m} \cos\left[\frac{2\pi R}{\lambda} \cos(\alpha + n\phi)\right] + i \sum_{n=-m}^{n=m} \sin\left[\frac{2\pi R}{\lambda} \cos(\alpha + n\phi)\right] \right|$$

where m is an integer, $2m + 1$ is the number of point sources, and ϕ is the angle subtended between any two adjacent point courses.

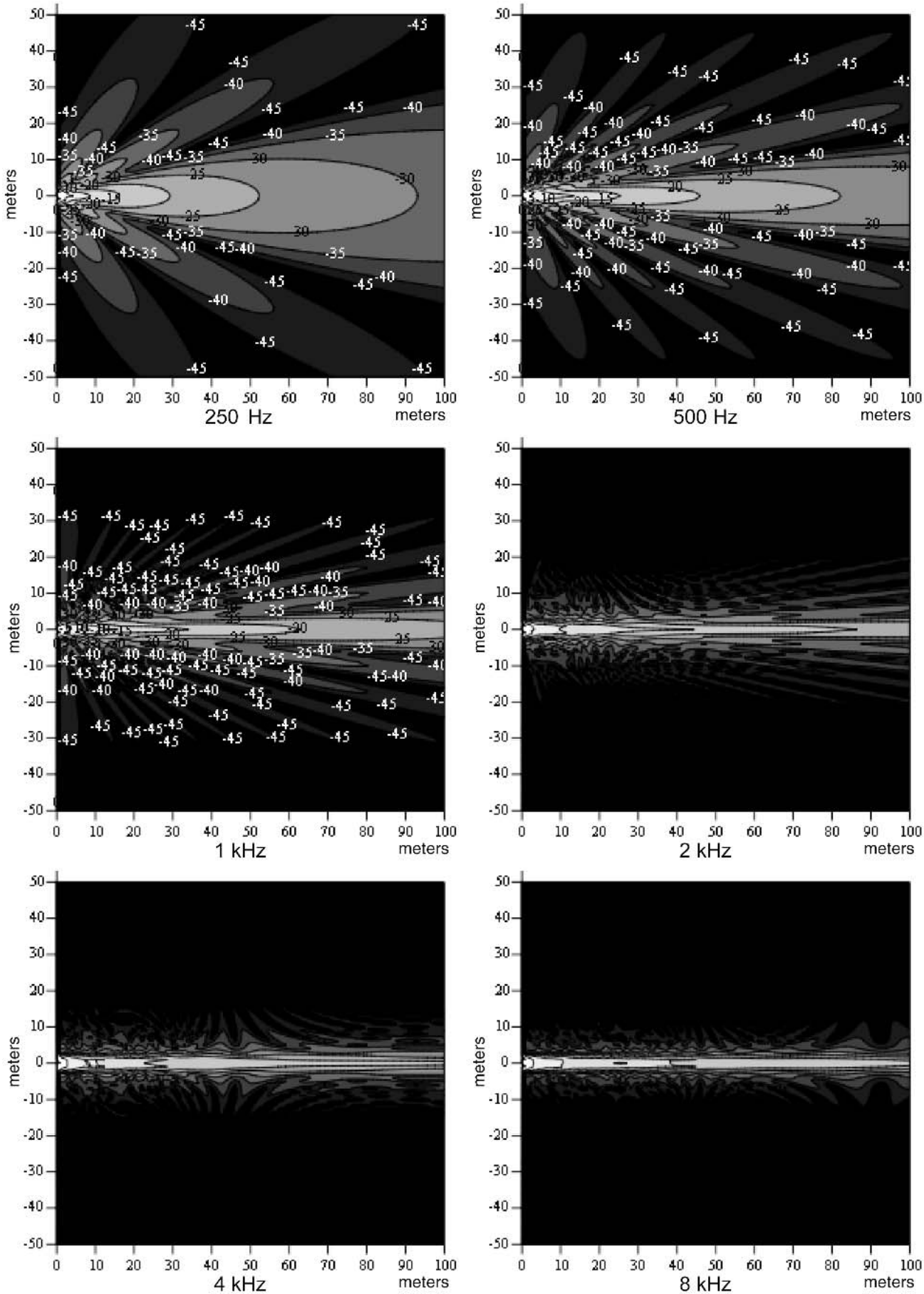

Fig. 13. Pressure fields of a 4-m line source. Contour scale numbers are removed from 2-, 4-, and 8-kHz plots for clarity.

where r_A is as expressed before. The polar response curves of a uniform 60° arc source at various ratios of radius and wavelength are shown in Fig. 15. In general these are wide for low ratios of $\boldsymbol{R}/\lambda$ and approach the included angle of the arc at higher ratios.

3.2 On-Axis Pressure Response of Arc Sources

The on-axis pressure response of an arc source can be expressed in a form similar to the earlier expressions for straight-line sources. Fig. 16 shows the geometric construction of an arc source with radius $\boldsymbol{R}$ and total included angle θ. The pressure of an arc source at distance x is

$$p_A(x) = \int_{-\theta/2}^{\theta/2} \frac{A(\phi)\, e^{-j[kr_A(x,\,\phi)+\varphi(\phi)]}}{r_A(x,\,\phi)} \boldsymbol{R}\, d\phi$$

where

$$r_A(x,\,\phi) = \sqrt{[x + \boldsymbol{R}(1-\cos\phi)]^2 + \boldsymbol{R}^2 \sin^2\phi}.$$

Fig. 17 provides a comparison of the pressure responses of equivalent-length uniform straight-line and arc sources. Though the arc source is curved only 30°, its on-axis response is materially smoother in the near field than the one produced by the straight-line source.

Like a line source, the pressure response of an arc source changes with the arc length and frequency. Fig. 18 shows the on-axis responses of three uniform arc sources of various lengths. The different lengths are provided by a constant radius (4 m) with an adjusted included angle. Fig. 19 shows how the pressure response changes with frequency. Note that the transition from the near field to the far field is generally smoother for an arc than for a line source at all lengths and frequencies.

3.3 Pressure Field of Arc Sources

The two-dimensional pressure field of an arc source is given by

$$p_A(x,\,y) = \int_{-\theta/2}^{\theta/2} \frac{A(\phi)\, e^{-j[kr_A(x,\,y,\,\phi)+\varphi(\phi)]}}{r_A(x,\,y,\,\phi)} \boldsymbol{R}\, d\phi$$

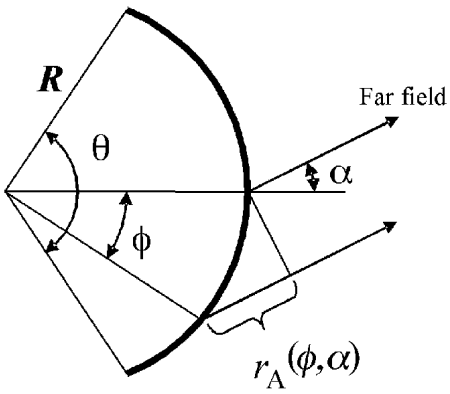

Fig. 14. Geometric construction of arc source for polar response.

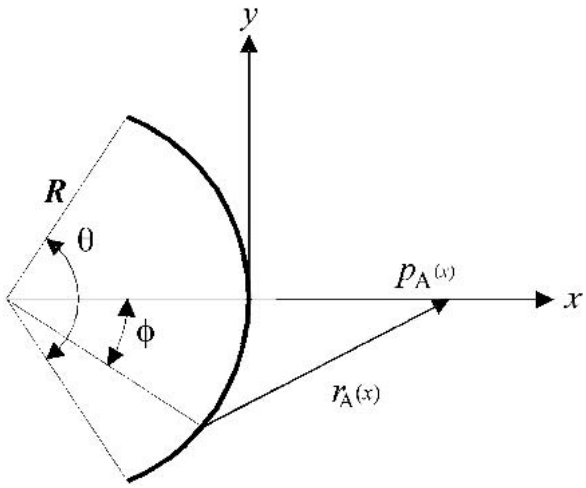

Fig. 16. Geometric construction of arc source for on-axis response.

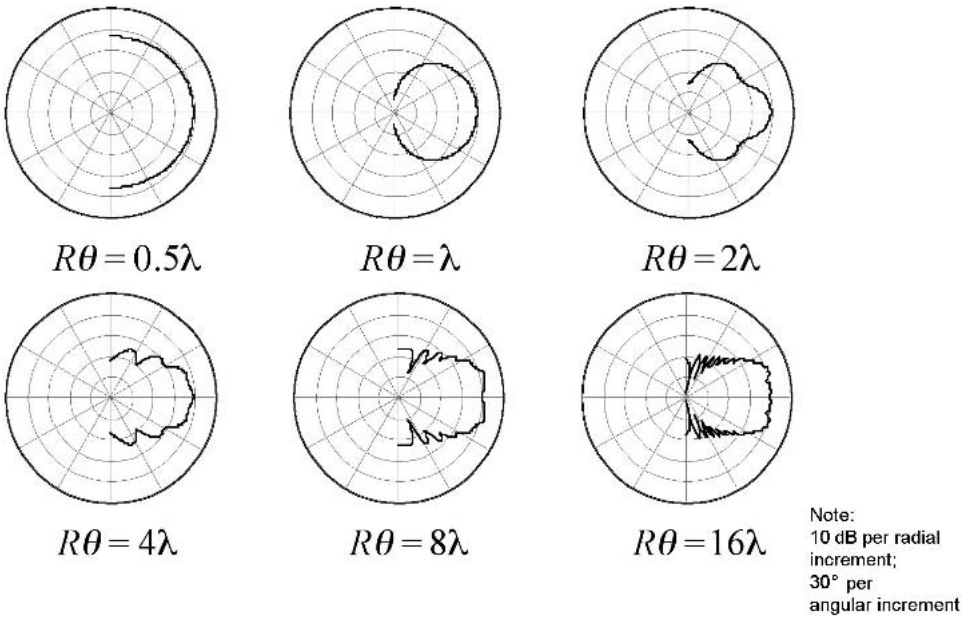

Fig. 15. Polar response curves of arc source.

where

$$r_A(x, y, \phi) = \sqrt{[x + R(1 - \cos\phi)]^2 + (y - R\sin\phi)^2}.$$

The geometric construction is shown in Fig. 20. Fig. 21 shows the pressure field of a uniform arc source, where $A(\phi) = A$ and $\varphi(\phi) = 0$, in several frequency bands. The response is quite different from that produced by a uniform straight-line source. At low frequency a uniform arc source can produce either a lobe or a null on axis. At mid and high frequencies a wedge pattern is produced that corresponds to the included angle of the arc.

4 SOURCES

A J source is comprised of a line source and an arc source. In general the straight segment is located above the arc segment and is intended to provide the long-throw component of the polar response. The arc segment is intended to provide coverage in the area below and in front of the source. Together the segments provide an asymmetric polar response in the vertical plane.

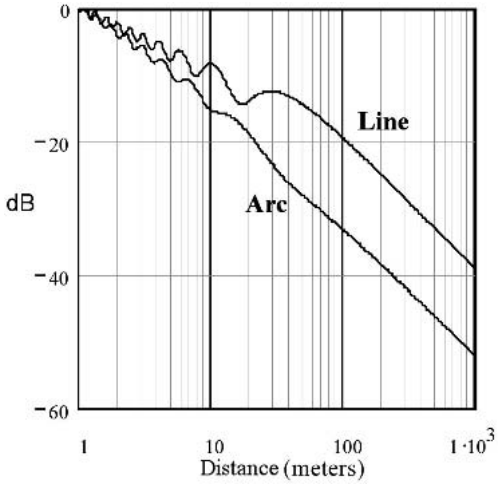

Fig. 17. On-axis pressure response of an arc source and a straight-line source at 4 kHz. Arc source has an included angle of 45° and a radius of 4 m. Line source has a length equal to the arc length (3.14 m).

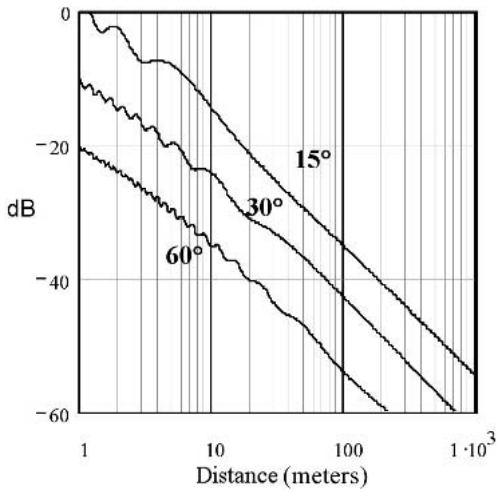

Fig. 18. On-axis pressure response of three arc sources (θ = 15, 30, and 60°) at 8 kHz where R = 4 m. These correspond to arc lengths of approximately 1, 2, and 4 m. The 30 and 60° curves are offset by 10 and 20 dB, respectively.

4.1 Polar Response of J Sources

The directivity function of a J source is obtained by combining the directivity functions of the line and arc sources presented in previous sections. The geometric construction is shown in Fig. 22, where L is the length of the straight segment and R and θ specify the arc segment. We assume that the straight and arc segments are adjacent and that the center point of the arc is on a line perpendicular to the straight segment through its lower endpoint.

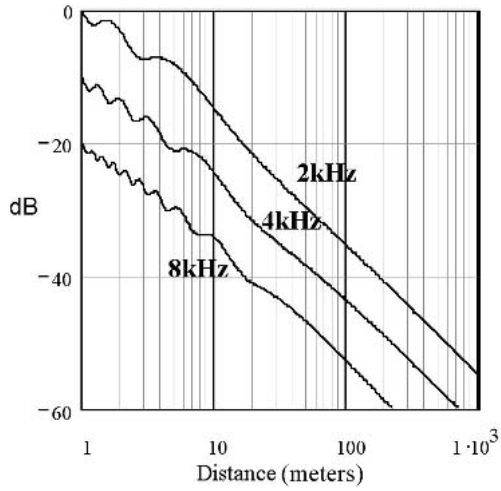

Fig. 19. On-axis pressure response of an arc source at various frequencies (θ = 30° and R = 4 m). The arc length is approximately 2 m. The 2- and 8-kHz curves are offset by 10 and 20 dB, respectively.

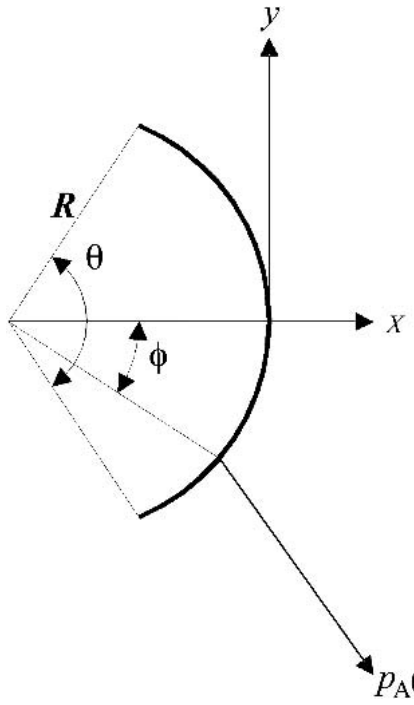

Fig. 20. Geometric construction for arc source pressure field.

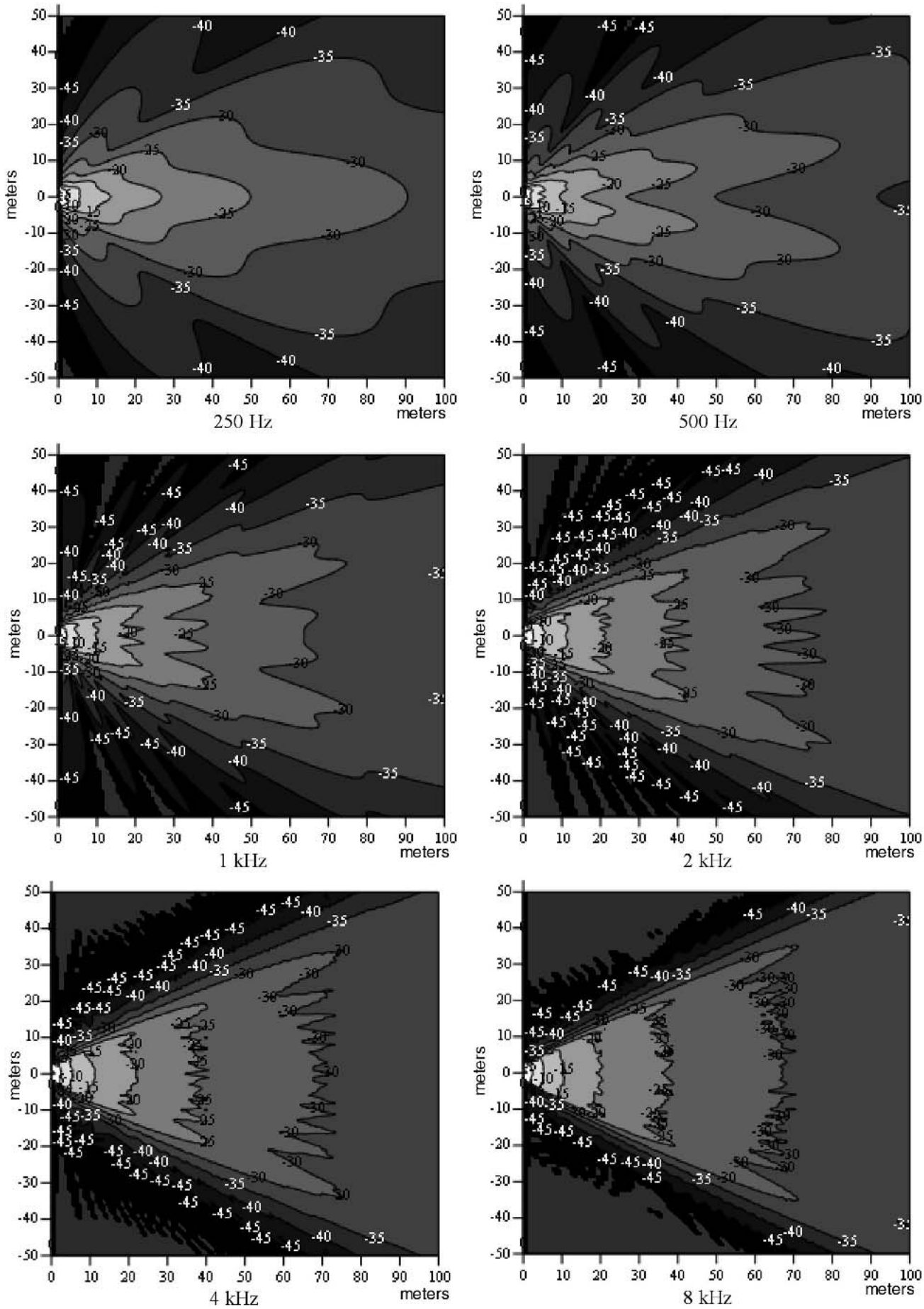

Fig. 21. Pressure fields of uniform arc source.

If we choose the center point of the line segment as the origin, then the pressure radiated from the line segment in the far field at off-axis angle α is

$$p_L(\alpha) = \frac{1}{r}\int_{-L/2}^{L/2} A_L(l)\, e^{-j[kr_L(\alpha, l)+\phi_L(l)]}\, dl$$

where

$$r_L(\alpha, l) = l \sin \alpha$$

as shown in Section 2.1. Here $A_L(l)$ and $\varphi_L(l)$ are the amplitude and phase functions of the line segment. Now since we must rotate the arc segment by θ/2 relative to the horizontal, we will also change the limits of integration. The pressure radiated in the far field from the rotated arc source is

$$R_A(\alpha) = \frac{1}{r}\int_0^{\theta} A_A(\phi)\, e^{-j[kr_A(\alpha, \phi)+\varphi_A(\phi)]}\boldsymbol{R}\, d\phi$$

where

$$r_A(\alpha, \phi) = 2\boldsymbol{R} \sin\left(\frac{\phi}{2}\right) \sin\left(\frac{\phi}{2} + \alpha\right)$$

and $A_A(\phi)$ and $\varphi_A(\phi)$ are the amplitude and phase functions of the arc segment. To properly sum the radiated pressure from the line and arc segments, a new function is required to express the relative distance difference between them. Referring to Fig. 22, it is given as

$$r_J(\alpha) = \frac{L}{2} \sin \alpha.$$

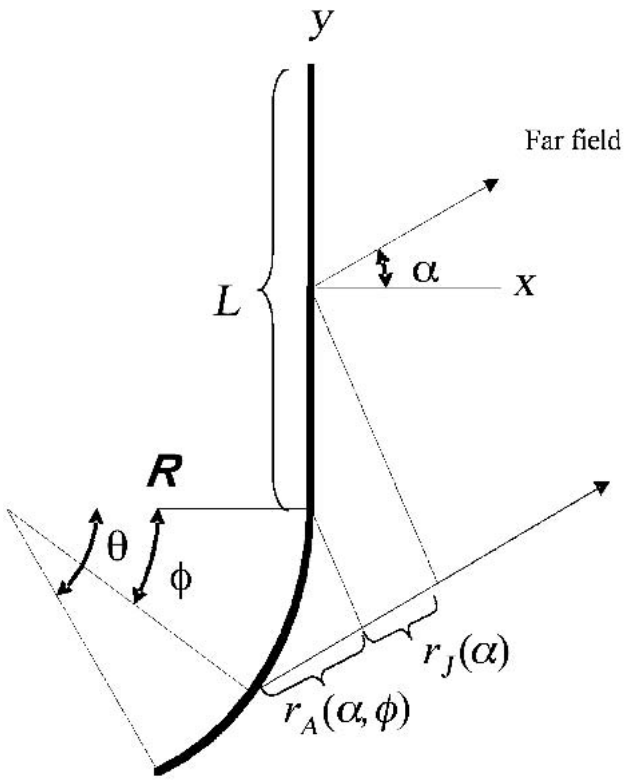

Fig. 22. Geometric construction of a J source for polar response.

The general form for the radiated pressure in the far field of a J source is then

$$p_J(\alpha) = \frac{1}{r}\left[\int_{-L/2}^{L/2} A_L(l)\, e^{-j[kr_L(\alpha, l)+\varphi_L(\phi)]}\, dl + \int_0^{\theta} A_A(\phi)\, e^{-j[kr_A(\alpha, l)+\varphi_A(\phi)+r_J(\alpha)]}\boldsymbol{R}\, d\phi\right].$$

If we assume that the amplitudes per unit length are uniform over the line and arc segments, and that the phase shifts are zero, the relative source strengths are proportional to their relative lengths. Letting A_L and A_A be the constant amplitudes per unit length of the line and arc segments, respectively, the directivity function of a J source reduces to

$$R_J(\alpha) = \frac{1}{A_L L + A_A \boldsymbol{R}\theta}\left|A_L\int_{-L/2}^{L/2} e^{-jkr_L(\alpha, l)}\, dl + A_A\int_0^{\theta} e^{-jk[r_A(\alpha, \phi)+r_J(\alpha)]}\boldsymbol{R}\, d\phi\right|.$$

The contributions of the line segment and the arc segment to the polar response of a uniform J source are shown in Fig. 23. As expected, the line segment provides a long throw and the arc segment provides a relatively wide angle of coverage rotated downward. The response of the J source is a blend of the two.

The polar response of a J source changes with the length of the line segment, the radius and included angle of the arc segment, the relative amplitudes of the two segments, and frequency. Fig. 24 shows polar response curves of a J source with a 2-m-long line segment, a 1-m radius, a 60° included angle, and equal amplitudes per unit length. The polars show that the straight segment of the J source dominates the response and produces a very narrow beam, particularly at high frequency. The arc segment does not fully balance the high gain of the straight segment.

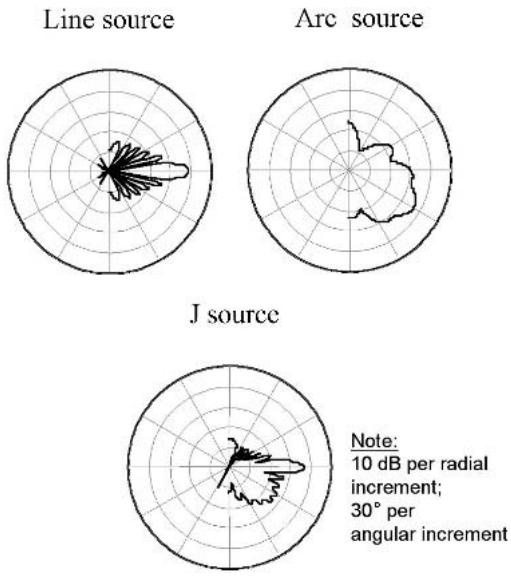

Fig. 23. Contribution of a line and an arc source to the polar response of a J source.

There are several approaches to providing a more balanced response. One is to make the straight segment shorter, thereby reducing the gain. A second is to increase A_A relative to A_L. For instance, one might use a J source that has a 1-m-long straight segment (as opposed to 2 m in the previous example) and set $A_A = 2A_L$ (instead of $A_A = A_L$). The polar response of this modified J source is considerably more balanced than the uniform J source, as shown in Fig. 25.

4.2 On-Axis Pressure Response of J Sources

The on-axis pressure response of a J source is obtained by combining the pressure response functions of the line and arc sources presented in the preceding. The geometric construction is shown in Fig. 26, where L is the length of the straight segment, and $\boldsymbol{R}$ and θ specify the arc segment. Note that the lower endpoint of the arc segment is taken as the initial point for the on-axis response. Based on this geometry, the pressure radiated at point $\boldsymbol{P}$ from a J source is

$$p_J(x) = \int_0^L \frac{A_L(l)\, e^{-j[kr_L(x,\, l)+\varphi_L(l)]}}{r_L(x,\, l)}\, dl + \int_0^\theta \frac{A_A(\phi)\, e^{-j[kr_A(x,\, \phi)+\varphi_A(\phi)]}}{r_A(x,\, \phi)}\, \boldsymbol{R}\, d\phi$$

where

$$r_L(x,\, l) = \sqrt{x^2 + (\boldsymbol{R} \sin\theta + l)^2}$$

$$r_A(x,\, \phi) = \sqrt{[x + \boldsymbol{R}(1 - \cos\phi)]^2 + \boldsymbol{R}^2(\sin\theta - \sin\phi)^2}.$$

Fig. 27 compares the on-axis pressure responses of uniform equivalent-length straight-line and J sources, where $A(\phi) = A$. The straight segment of the J source dominates the response, producing undulations in the near field very similar to those of the straight-line source. However, the on-axis aperture of the J source is foreshortened relative to the equal-length line source, so the distance to the far field is marginally shorter.

4.3 Pressure Field of J Sources

The geometric construction for the pressure field of a J source is shown in Fig. 28. The general form for the pressure at $\boldsymbol{P}$ is

$$p_J(x,\, y) = \int_0^L \frac{A_L(l)\, e^{-j[kr_L(x,\, y,\, l)+\varphi_L(\phi)]}}{r_L(x,\, y,\, l)}\, dl + \boldsymbol{R}\int_0^\theta \frac{A_A(\phi)\, e^{-j[kr_A(x,\, y,\, \phi)+\varphi_A(\phi)]}}{r_A(x,\, y,\, \phi)}\, d\phi$$

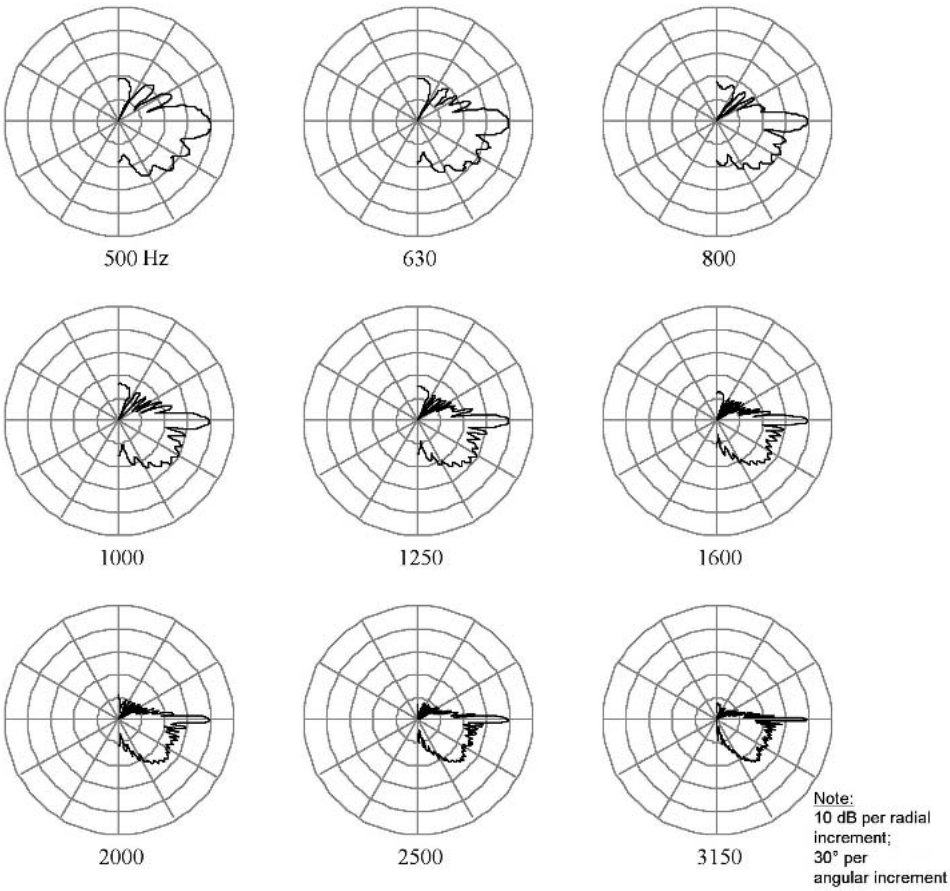

Fig. 24. J-source polar response curves (Example 1). $L = 2$ m, $R = 1$ m, $\theta = 60°$, $A_L = 1$, $A_A = 1$.

where

$$r_L(x, y, l) = \sqrt{x^2 + (y + l)^2}$$

$$r_A(x, y, \phi) = \sqrt{[x + R(1 - \cos\phi)]^2 + (y + L + R\sin\phi)^2}.$$

The pressure field of a uniform J source, where $A(\phi) = A$ and $\varphi(\phi) = 0$ in several frequency bands, is shown in Fig. 29. The parameters of the J source are the same as those used for the modified J source described in Section 4.1, that is, a 1-m straight segment and $A_A = 2A_L$. These plots show clearly that a J source is a blend of straight and arc sources. This is particularly true at mid and high frequencies, where the constituent responses are easily identifiable.

5 PROGRESSIVE SOURCES

Like a J source, a progressive source provides an asymmetric polar response in the vertical plane. However,

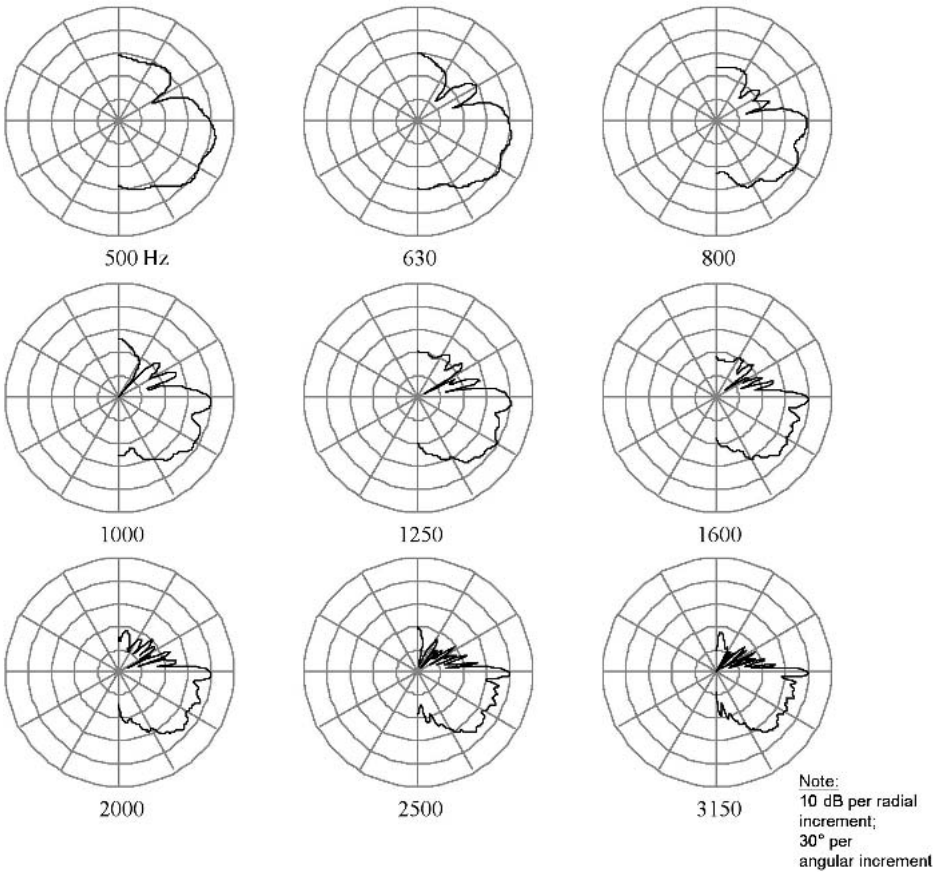

Fig. 25. J-source polar response curves (Example 2). $L = 1$ m, $R = 1$ m, $\theta = 60°$, $A_L = 1$, $A_A = 2$.

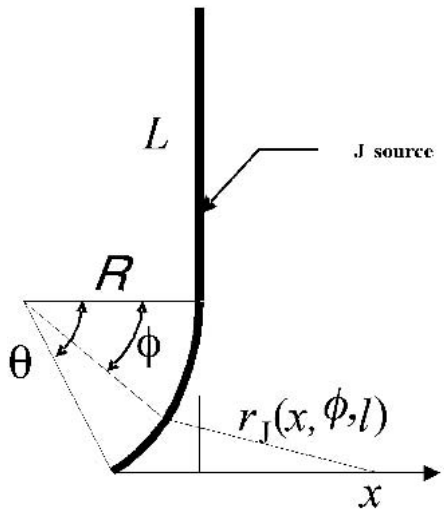

Fig. 26. Geometric construction of a J source for on-axis pressure response.

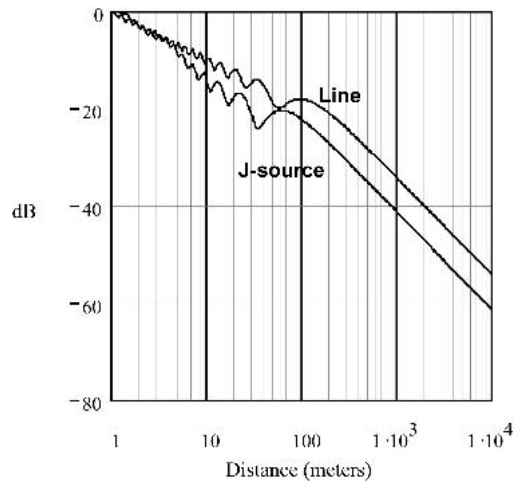

Fig. 27. Comparison at 2 kHz of on-axis pressure response of a 4-m-long straight-line source and a J source. $L = 2$ m, $R = 2$ m, $\theta = 60°$, $A_L = 1$, $A_A = 1$.

unlike a J source, it is a continuous curve rather than two distinct segments. The curvature increases with the distance along the curve. This results in an upper portion that is largely straight and a lower portion that is curved downward.

5.1 Polar Response of Progressive Sources

There are numerous possible mathematical expressions for progressive expansions, each providing different rates of curvature. The relevant set of expressions for loudspeaker arrays is characterized by curvature changes at equal intervals of length along the progressive curve. The interval corresponds to the height of a single loudspeaker enclosure of the array.

An arithmetic progressive source is one for which the angle between successive enclosures changes by a predetermined angle given by $(n - 1)\Delta\theta$, where n is the nth enclosure and $1 < n < N$, with N being the total number of enclosures in the array. For example, if $\Delta\theta = 1°$ and the first enclosure is hung at 0° (horizontal), the second enclosure would be hung at 1° relative to the first enclosure and the third at 2° relative to the second enclosure. This defines a progressive curve, here the aiming angle of the nth enclosure is oriented to the horizontal axis by 0°, 1°, 3°, 6°, 10°, and so on—an arithmetic expansion. An incremental angle $\Delta\theta$ of 2° would yield 0°, 2°, 6°, 12°, and 20°. The terminal angle Ω of an array, that is, the aiming angle relative to the horizontal of the last enclosure, is given by

$$\Omega = \frac{1}{2} N(1 + N)\Delta\theta$$

where N is the total number of enclosures. The total length of the source is

$$L = NH$$

where H is the height of a single enclosure. These two terms, Ω and L, fully define an arithmetic progressive source.

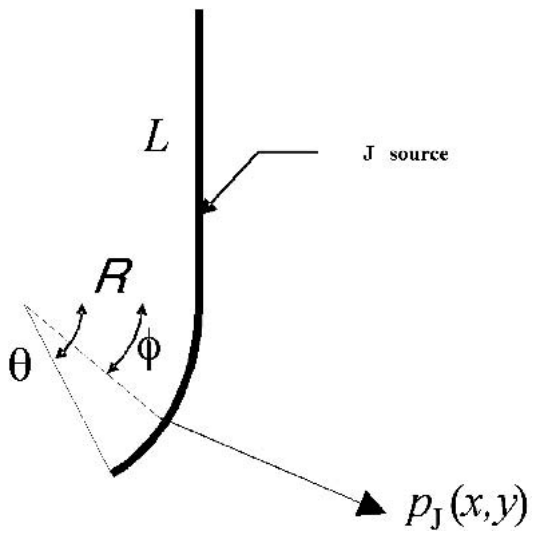

Fig. 28. Geometric construction for pressure field of a J-source.

The far-field directivity function of an arithmetic progressive source is derived in the same manner as used earlier for the line, arc, and J sources. The pressure radiated along the source is summed at a point ***P*** in the far field. The shape of the polar response curves will be determined primarily by the small distance function r_S.

The first step is to express the progressive source as a continuum of small radiating segments of length ΔL. ΔL should be chosen to be a small fraction of the shortest wavelength of interest. As a practical guideline, ΔL should be set approximately equal to one-quarter of a wavelength, that is,

$$\Delta L = \frac{\lambda}{4}.$$

The total number of segments is then

$$M = \frac{L}{\Delta L}$$

and the incremental angle between the element is

$$\Delta\psi = \frac{2\Omega}{M(M + 1)}.$$

The progressive source can then be expressed in parametric form as

$$x(\sigma) = \sum_{\eta=0}^{\sigma} -\sin\left[\frac{1}{2\eta(\eta + 1)}\Delta\psi\right]\Delta L$$

$$y(\sigma) = \Delta L + \sum_{\eta=0}^{\sigma} -\cos\left[\frac{1}{2\eta(\eta + 1)}\Delta\psi\right]\Delta L.$$

The geometric construction of an arithmetic progressive source is shown in Fig. 30. Its far-field directivity function is

$$R_S(\alpha) = \frac{\left|\sum_{\sigma=0}^{M} A_\sigma\, e^{-j[kr_S(\sigma,\,\alpha)+\varphi_\sigma]}\right|}{\left|\sum_{\sigma=0}^{M} A_\sigma\right|}$$

where

$$r_S(\sigma, \alpha) = \sin\left[\alpha - \tan^{-1}\left(\frac{x(\sigma)}{y(\sigma)}\right)\right]\sqrt{x(\sigma)^2 + y(\sigma)^2}.$$

The far-field directivity function for a uniform progressive source, where $A_\sigma = A$ and $\varphi_\sigma = 0$, is

$$R_S(\alpha) = \frac{1}{M + 1}\left|\sum_{\sigma=0}^{M} e^{-jkr_S(\sigma,\,\alpha)}\right|$$

where r_S was given before. The polar response of a uniform arithmetic progressive source is remarkably constant with frequency. Fig. 31 shows the polar response curves of a 5-m-long progressive source with a terminal angle of 45°.

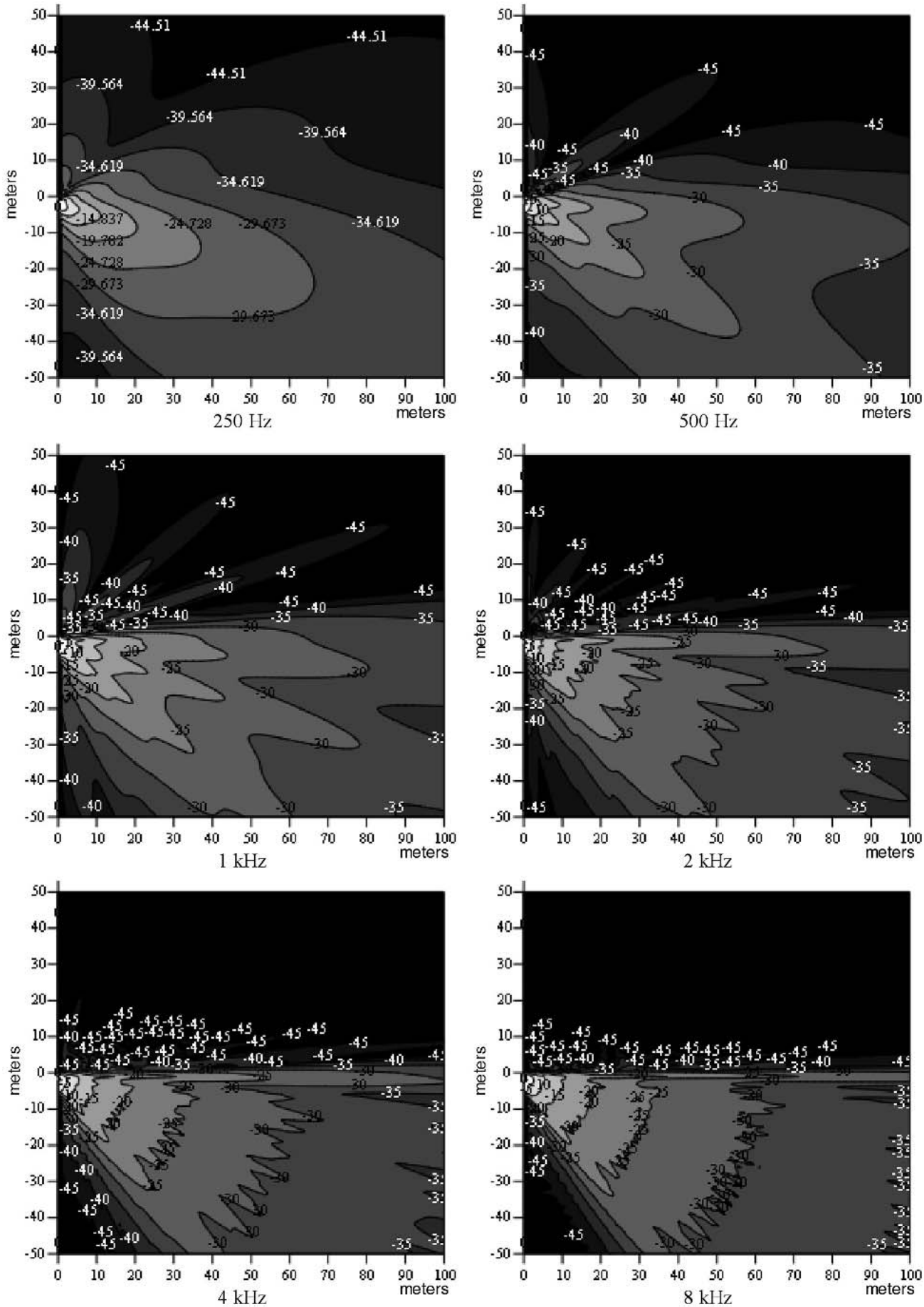

Fig. 29. Pressure field of a J source versus frequency.

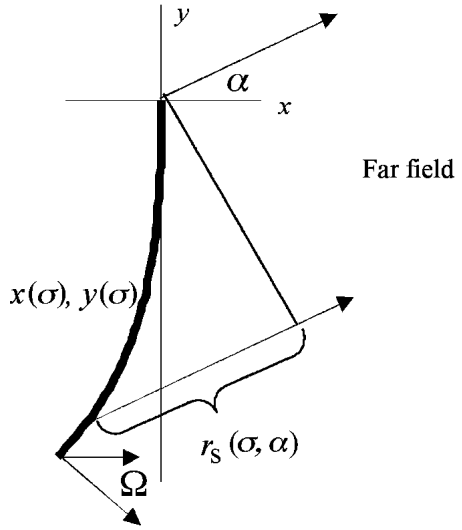

Fig. 30. Geometric construction of a progressive source for polar response.

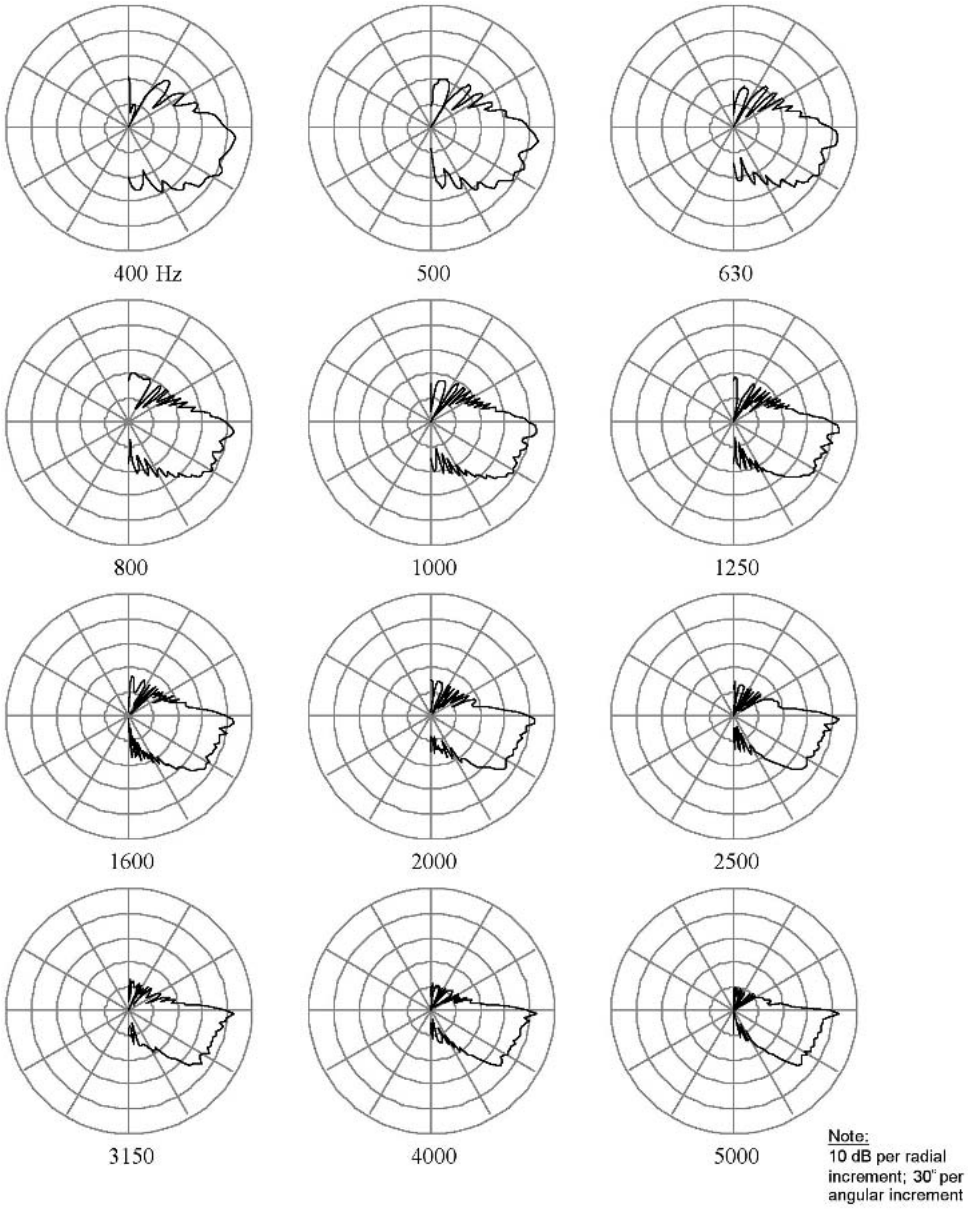

Fig. 31. Polar response of a 5-m-long progressive source with 45° terminal angle.

5.2 On-Axis Pressure Response of Progressive Sources

The geometric construction for the on-axis pressure response of a progressive source is shown in Fig. 32. The pressure response along a path from the lower end is

$$p_S(x) = \sum_{\sigma=0}^{M} A_\sigma \frac{e^{-j[kr_S(x,\,\sigma)+\vartheta_\sigma]}}{r_S(x,\,\sigma)}$$

where

$$r_S(x,\,\sigma) = \sqrt{[x - x(\sigma)]^2 + [y(M) - y(\sigma)]^2}$$

and A_σ is the amplitude at element σ and φ_σ is the relative phase at element σ.

Fig. 33 compares the on-axis response curves of equivalent-length uniform straight-line and progressive sources. These curves show that the progressive source has reduced undulations in the near field and a smoother transition from the near field to the far field.

5.3 Pressure Field of Progressive Sources

The geometric construction for the pressure field of a progressive source is shown in Fig. 34. The pressure at any point ***P*** is

$$p_S(x,\,y) = \sum_{\sigma=0}^{M} A_\sigma \frac{e^{-j[kr_S(x,\,y,\,\sigma)+\vartheta_\sigma]}}{r_S(x,\,y,\,\sigma)}$$

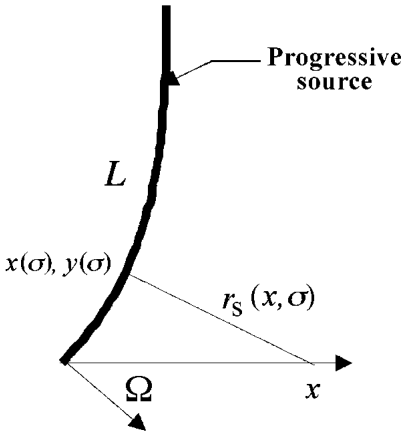

Fig. 32. Geometric construction of a progressive source for on-axis pressure response.

where

$$r_S(x,\,y,\,\sigma) = \sqrt{[x - x(\sigma)]^2 + [y - y(\sigma)]^2}.$$

The pressure field of a uniform progressive source in several frequency bands is shown in Fig. 35. These results illustrate the well-behaved asymmetrical response of a progressive source that makes them an excellent geometry upon which to base loudspeaker arrays for sound-reinforcement applications.

6 ADVANCED TOPICS

As a practical matter, large line arrays of loudspeakers are not perfectly continuous line sources. For instance, they may have gaps between the loudspeaker enclosures because of enclosure construction material or spacing. These gaps are effectively nonradiating portions of the line and may have an effect on the performance of the array. Also, certain radiating elements in loudspeaker line arrays may produce radial wavefronts instead of pure, flat wavefronts. This may also have an effect on the performance of the array. These topics are analyzed in the following sections.

6.1 Gaps in Line Sources

In previous sections we assume that each type of line source is continuous along its entire length. In practice,

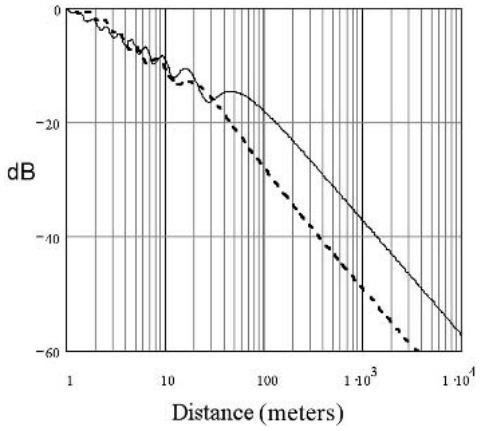

Fig. 33. Pressure response comparison at 2 kHz of a 45° terminal angle, 4-m-long progressive source and a line source of the same length.

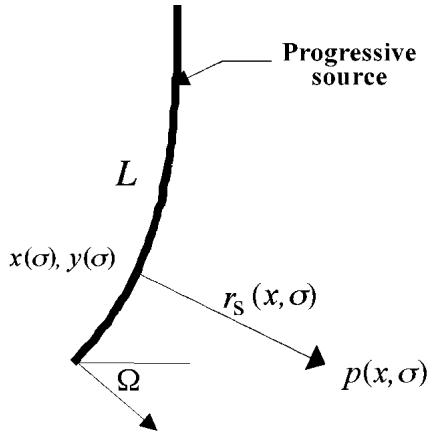

Fig. 34. Geometric construction for pressure field of a progressive source.

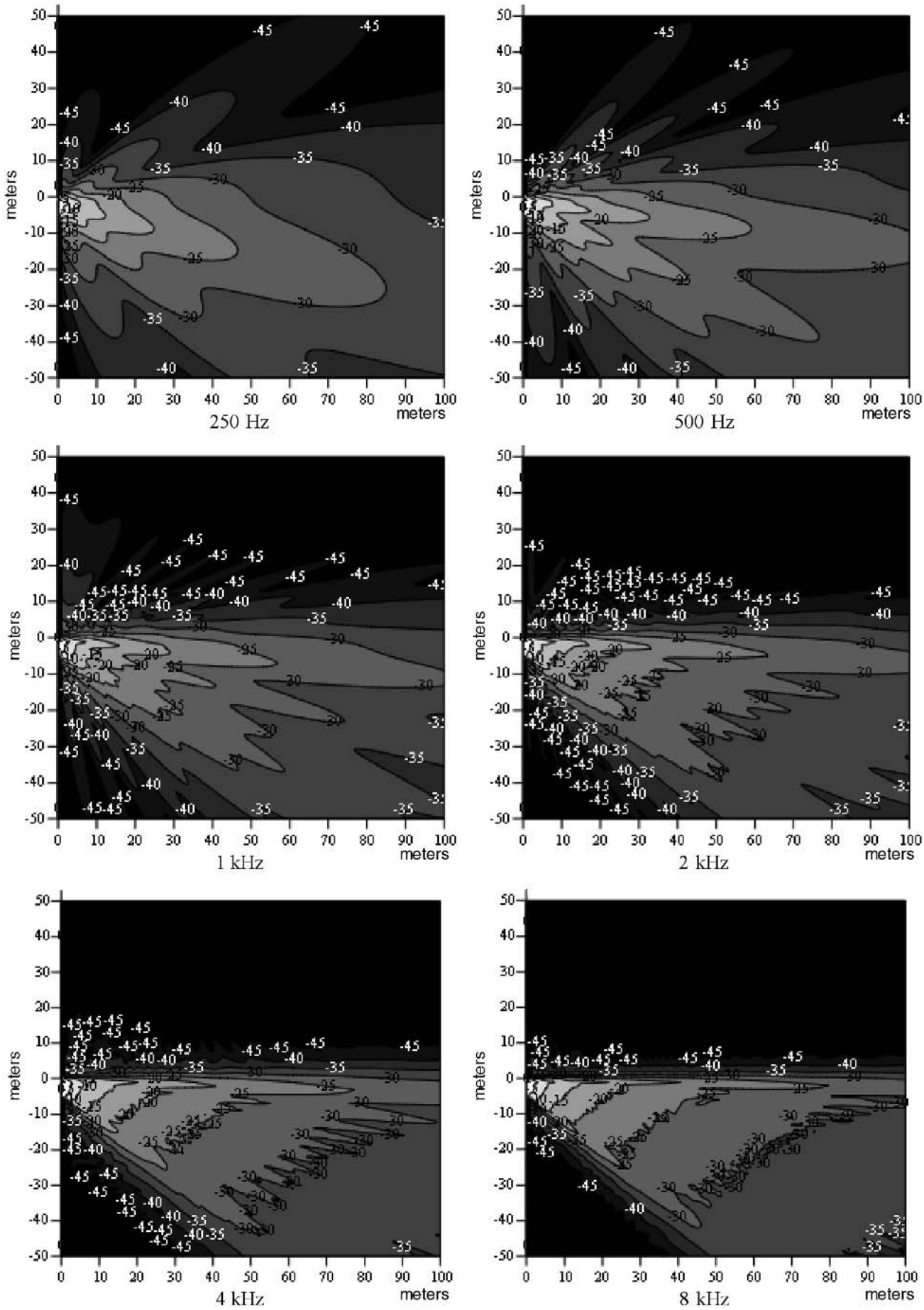

Fig. 35. Pressure fields of a progressive source versus frequency.

however, it may not be possible to achieve this. For instance, the thickness of the material used to construct a loudspeaker enclosure does not radiate acoustic energy. When loudspeaker enclosures are stacked into an array, these nonradiating segments are distributed along the length of the array. This can be modeled by limiting the integration of the line source to the radiating portions only. Referring to Fig. 36, d is the dimension of the nonradiating element on either side of the radiating element.

The directivity function of a line source with N elements of length L and gaps between them is

$$R(\alpha) = \sum_{1}^{N} \frac{\left| \int_{(N-1)L+d}^{NL-d} A(l)\, e^{-j[kl \sin \alpha + \phi(l)]}\, dl \right|}{\left| \int_{(N-1)L+d}^{NL-d} A(l)\, dl \right|}.$$

In general, gaps have very little effect on the primary lobe but change the structure of the off-axis lobes and nulls. Fig. 37 shows the linear polar response[14] of a four-element uniform line source with gaps. The graphs show the effects of changing the radiating percentage from 100% to 90, 75, and 50%. At low frequency, where the gap length is a small fraction of the wavelength, gaps have very little effect. At high frequency, the sidelobe structure changes materially with the gap length. The lobes get wider and change position.

Contemporary loudspeaker line array enclosures are usually designed to maximize the radiating percentage. If an enclosure is 0.5 m high and constructed of typical materials, radiating percentages can exceed 90%. However, if the spacing between enclosures gets large, gaps may exceed this threshold and the polar response will be affected.

[14]Linear polar response is a rectilinear representation of the polar response, that is, dB along the y axis and angle along the x axis.

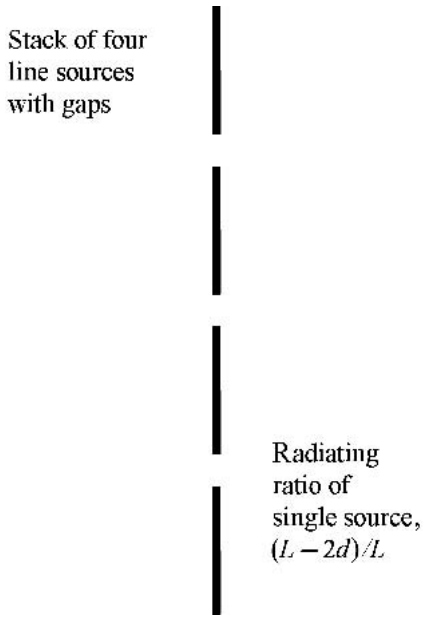

Fig. 36. Line array of four elements of length L and nonradiating gap d on either end.

6.2 Stack of Arc Sources versus Line Sources

In practice, certain components of a loudspeaker system may produce wavefronts that are curved instead of perfectly straight. When stacked in an array, these may more closely resemble a stack of arc sources rather than a continuous straight-line source. Fig. 38 shows a stack of three arc sources representing an array of three loudspeaker components with radial wavefronts. The effects that radial wavefronts have on the directivity function can be estimated by summing the radiation from a stack of arc sources.

As derived in Section 3.1, the directivity function of a

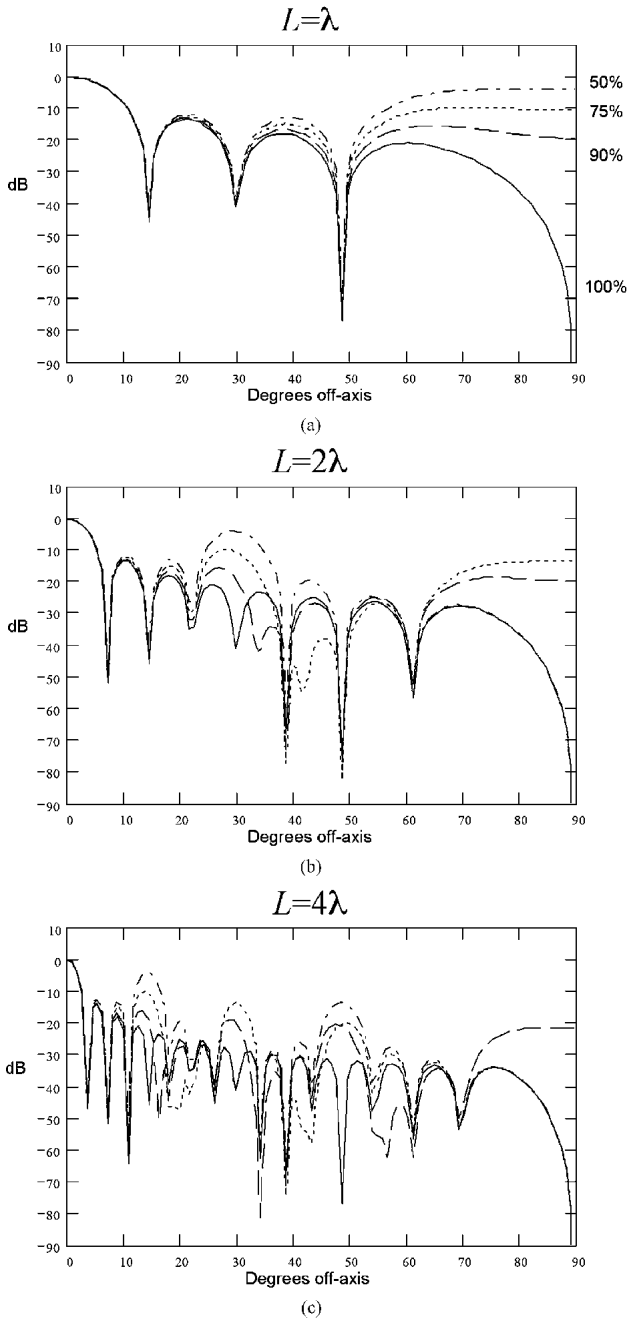

Fig. 37. Directivity function of four-element line array with four radiating percentages at three length-to-wavelength ratios. - · - 50%, --- 75%; –– 90%; —— 100%.

uniform arc source is

$$R_A(\alpha) = \frac{1}{\boldsymbol{R}\theta}\left|\int_{-\theta/2}^{\theta/2} e^{-jkr_A(\phi,\alpha)}\boldsymbol{R}\,d\phi\right|$$

where

$$r_A(\phi,\alpha) = 2\boldsymbol{R}\sin\left(\frac{\phi}{2}\right)\sin\left(\frac{\phi}{2}+\alpha\right).$$

Here $\boldsymbol{R}$ is the radius and θ the included angle of the arc. The directivity function of a stack of arc sources is obtained by applying the first product theorem.[15] In this case the directivity function of the arc is multiplied by the directivity function of an array of simple sources. The far-field directivity function for an array of N simple sources of equal amplitude and phase distributed a distance D apart along a line is given by

$$R_P(\alpha) = \frac{1}{N}\left|\sum_{n=1}^{N} e^{-j[k(n-1)D\sin\alpha]}\right|.$$

Applying the first product theorem, the directivity function of a vertical stack of arc sources is

$$R_{AP}(\alpha) = R_A(\alpha)R_P(\alpha).$$

Fig. 39 shows the effects of nonflat wavefronts on the directivity function of the sources, compared to a perfectly flat wavefront. As with gaps in a line source, a curvature primarily produces changes in the lobe/null structure of the off-axis response. The changes increase with increasing curvature and are more predominant when the curvature is a material fraction of a wavelength.

Fig. 39(a) compares the directivity function of a uniform line source of length $3L$ with an array of three curved sources of length L, where the curvature δ of the arc is one-eighth wavelength. The directivity functions are very similar, with only small differences in the lobe/null struc-

[15]The first product theorem states that the directional factor of an array of identical sources is the product of the directional factor of the array and the directional factor of a single element of the array. See Kinsler et al. [20].

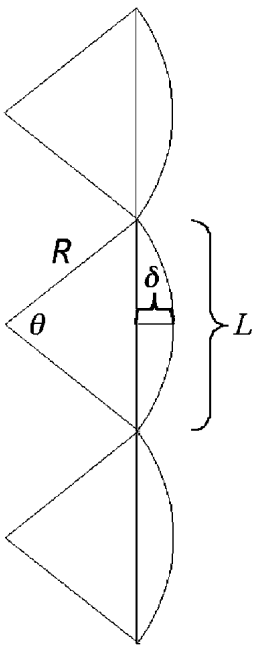

Fig. 38. Stack of three arc sources of radius $\boldsymbol{R}$, included angle θ, and curvature δ.

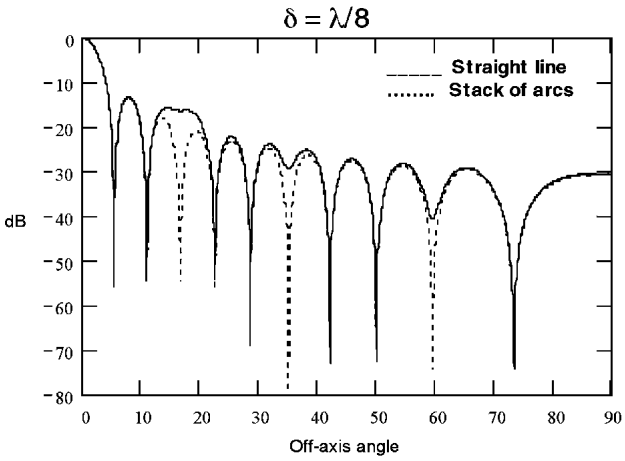

(a)

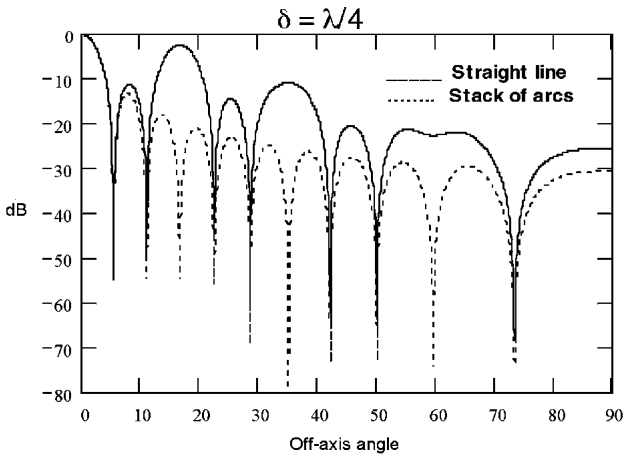

(b)

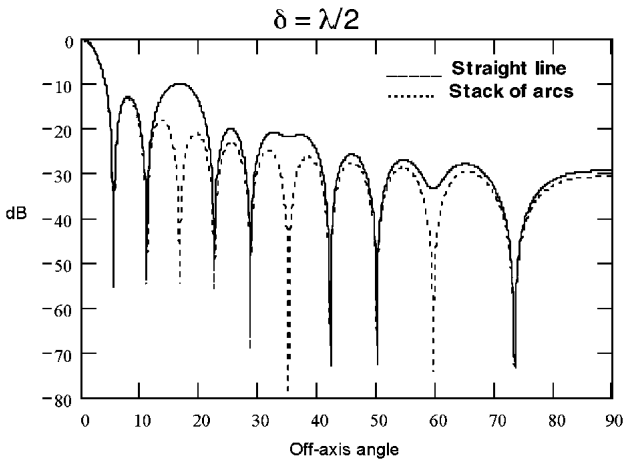

(c)

Fig. 39. Comparison of directivity functions of a stack of three curved sources and a straight-line source. Curved sources have element length L = 150 mm, total included angle θ = 20°. Straight-line source has total length $3L$.

ture. In particular, note that the nulls at approximately 18, 35, and 60° are not as deep with the stack of arc sources.

Fig. 39(b) and (c) shows the directivity functions of the uniform line and the three-element array at curvatures of one-quarter and one-half wavelengths. In these cases, lobes gradually replace the nulls at 18, 35, and 60°. At one-quarter wavelength the lobe at 18° is approximately 10 dB below the level of the on-axis lobe, up from approximately 20 dB. This represents a practical limit to the curvature, which maintains, generally speaking, the directivity function of a pure line source. The response at one-half wavelength is unacceptable as the 18° lobe is here nearly equal in amplitude to the primary lobe.

This one-quarter-wavelength limit on curvature allows us to estimate, for a given curvature, the practical upper frequency limit for which it maintains the directivity response of a uniform line source. If a source has an element length L of 130 mm and a total arc angle of 20°, then

$$\delta = \frac{L}{2}\tan\left(\frac{\theta}{4}\right) = 6.6 \text{ mm}$$

and the upper frequency limit is

$$f = \frac{c}{4\delta} \approx 13 \text{ kHz}.$$

Polar response curves of a stack of three 150-mm-high, 20° sources are shown in Fig. 40. The data are superimposed over the polar response of a line source 450 mm long. The 20° source tends to merge the third and fourth off-axis lobes. The amplitude of this merged lobe increases with frequency. At approximately 12.5 kHz the lobes are 10 dB below the primary on-axis lobe. This corresponds closely to the 13 kHz estimate given earlier.

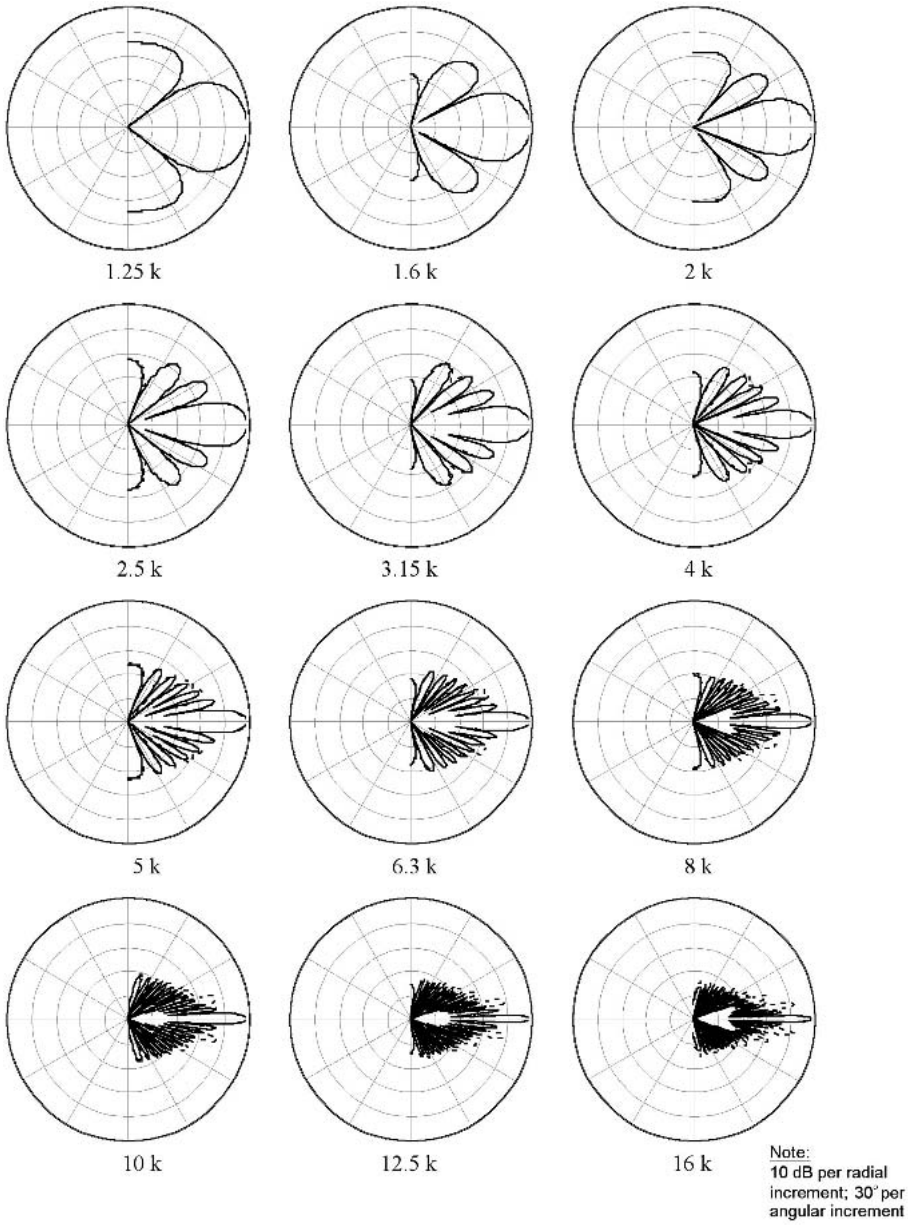

Fig. 40. Polar response curves of a stack of three 150-mm-high, 20° arc sources (- - -) superimposed over response of a 450-mm straight-line source (——).

7 APPLICATIONS

The mathematical models developed in the previous sections will provide useful estimates of the performance of many types of loudspeaker line arrays. However, the accuracy of the estimates may be compromised by several factors. First, real-life loudspeaker systems do not often behave like perfect sources. In addition to the gaps and radial wavefronts discussed in Section 6, other potential factors include cone or diaphragm breakup, suspension and magnetic nonlinearities, and enclosure resonance and edge (diffraction) effects. Second, collecting far-field data can be problematic since the microphone must be placed at large distances. Most anechoic chambers provide adequate distances to measure only relatively small arrays. Large arrays can be measured outdoors, but environmental factors such as wind and atmospheric turbulence may affect results. Alternatively, data may be taken in a large indoor space, but the acoustical characteristics of the room must be isolated and removed from the measurements. Nonetheless, despite all of these potential sources of errors, useful estimates can be produced, as illustrated in the following examples.

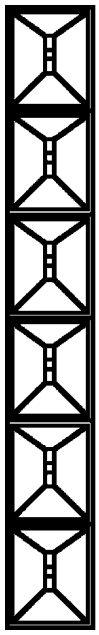

Fig. 41. Vertical stack of six 8-in (203-mm)-tall, 40° by 20° horns.

7.1 Example 1: Small Straight-Line Array—Low-Frequency Model

The first example compares the modeled polar response of a small straight-line array against measured results. The array is comprised of six small horns stacked in a vertical array, as shown in Fig. 41. Each horn is approximately 8 in (203 mm) tall, resulting in an array 48 in (1.22 m) high. Polar data were collected on this array at a distance of 15 ft (4.6 m) in an anechoic chamber. See Ureda [21].

The most straightforward approach to model this array is to assume that it is a uniform straight-line source. This assumption will hold at low frequency, where the mouth is less than one wavelength high. Since this horn has a mouth[16] height of approximately 6.5 in (165 mm), the highest usable frequency of the model is approximately 2 kHz. From Section 2.2 the directivity function of a uniform line source is

$$R_U(\alpha) = \frac{1}{L}\left|\int_{-L/2}^{L/2} e^{-jkl\sin\alpha}\, dl\right|$$

where in this case $L = 48$ in (1.22 m). Fig. 42 shows measured versus modeled polar responses. Note that the model assumes a sine wave input that yields a very fine

[16]The horn is 8 in (203 mm) tall, but the mouth is only 6.5 in (165 mm) because mounting flanges on either side of the mouth are 0.75 in (19 mm) wide.

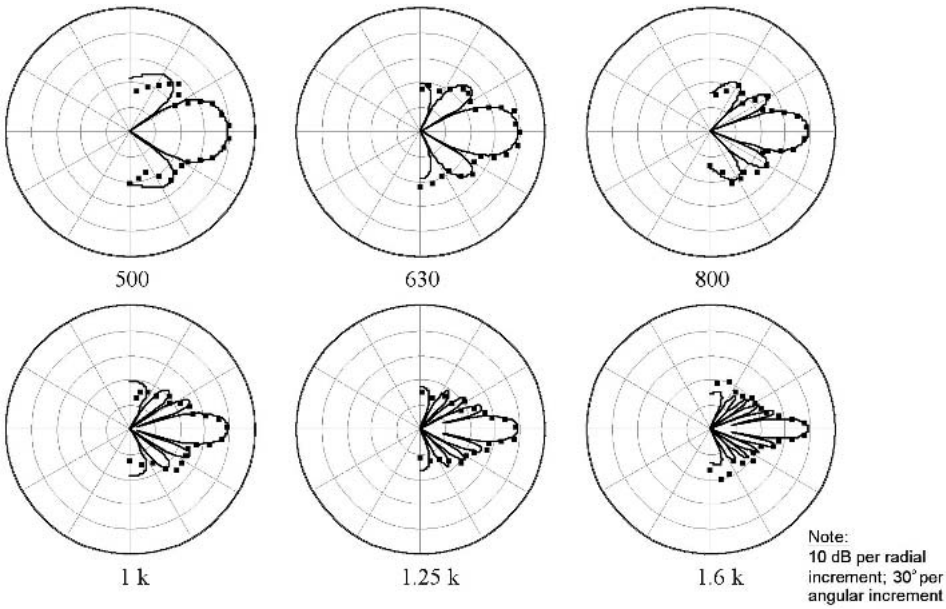

Fig. 42. Measured (· · ·) versus modeled (——) polar response curves of array in Fig. 41. Model based on a uniform straight-line source with a sine wave input. Measured data are one-third-octave pink noise.

lobe and null structure. The measured data are one-third-octave pink noise, which tends to fill the sharp nulls of a sine wave response. Nonetheless, the modeled response closely resembles the measured data. Note that the 1.5-in (38-mm) gaps between the horn mouths do not materially affect the modeled performance.

7.2 Example 2: Small Straight-Line Array—High-Frequency Model

The polar response estimate of the six-horn array described in Section 7.1 can be extended to higher frequencies, if we use a stack of arc sources instead of a uniform straight-line model. This is reasonable since the polar response of the individual horns will approach the vertical coverage angle at higher frequency. The horns have a vertical coverage angle of 20°. Using the directivity function of a stack of uniform arc sources from Section 6.2, where

$$R_{AP}(\alpha) = R_A(\alpha)R_P(\alpha)$$

$$R_P(\alpha) = \frac{1}{N}\left|\sum_{n=1}^{N} e^{-j[k(n-1)D\sin\alpha]}\right|$$

$$R_A(\alpha) = \frac{1}{\boldsymbol{R}\theta}\left|\int_{-\theta/2}^{\theta/2} e^{-jkr_A(\phi,\alpha)}\boldsymbol{R}\,d\phi\right|$$

$$r_A(\phi,\alpha) = 2\boldsymbol{R}\sin\left(\frac{\phi}{2}\right)\sin\left(\frac{\phi}{2}+\alpha\right)$$

$$\boldsymbol{R} = \frac{L}{2\sin\left(\frac{\theta}{2}\right)}$$

and setting $N = 6$, $L = 6.5$ in (165 mm), $D = 8$ in (203 mm), and $\theta = 20°$, we obtain the polar response curves shown in Fig. 43. Again, the curves are based on a sine wave response, and the measured data were collected in one-third-octave bands of pink noise. Nonetheless the model predicts the grating lobes at the higher frequencies.

7.3 Example 3: Large Curved Array

Engebretson et al. [18] recently took polar response data on several large arrays. Among these was an eight-element curved array. Each element is approximately 0.5 m high, resulting in a total length of 4 m. Vertical polar data were derived from ground-plane MLSSA impulse measurements taken at 20 m on 5° intervals. The data were taken inside a vacant airplane hangar to prevent wind-borne temperature gradients and other disturbances. Fig. 44 shows the array of eight cabinets configured for ground-plane measurements. The eight boxes are shown set on end with 5° splay angles between adjacent cabinets.

This array can be modeled as an arc source with an included angle of 40° and an arc length of 4 m. The polar response at standard one-third-octave center frequencies can be estimated using the far-field directivity function of a uniform arc source. From Section 3.1, this is

$$R_A(\alpha) = \frac{1}{\boldsymbol{R}\theta}\left|\int_{-\theta/2}^{\theta/2} e^{-jkr_A(\alpha,\phi)}\boldsymbol{R}\,d\phi\right|$$

where

$$\boldsymbol{R} = \frac{L}{\theta}$$

and

$$r_A(\alpha,\phi) = 2\boldsymbol{R}\sin\left(\frac{\phi}{2}\right)\sin\left(\frac{\phi}{2}+\alpha\right).$$

The modeled polar response curves are shown in Fig. 45. The measured data from Engebretson et al. are shown as dots superimposed on the modeled curves. Note that the measured data are at 5° increments—the directivity function provides continuous curves. We can see that the agreement between measured and modeled is quite reasonable. The large lobes along the sides of the polars may be due to diffraction effects or room effects. Neither of these effects is accounted for in the model. Nonetheless, the model provides a useful estimate of the polar response across more than six octaves.

8 SUMMARY

This paper provides mathematical models that estimate the performance of several types of loudspeaker line arrays. Specifically, models are provided to estimate the polar response, on-axis pressure response, and pressure fields of straight, curved (arc), J, and progressive arrays. The first few sections provide a review of uniform straight-line sources, including derivations of the far field polar response, lobe and null structure, and quarter-power angle as a function of frequency. The remaining sections represent largely new work and are summarized as follows.

First, the pressure response of a line source as a function of distance is shown to be dependent on the path along which the response is calculated. Typically a path is taken normal to the source, beginning at its midpoint. This introduces symmetry into the model and produces a result that is unique to this origin and path. The paper illustrates how different responses are obtained by choosing alternate origins. The paper further notes that it is typical to use the midpoint of the source as the origin for the normal path to estimate the transition distance. This understates the complexity of the transition from the near field to the far field. The paper suggests using pressure fields instead of pressure response to fully capture this complexity and derives the required mathematical expressions.

Second, J and progressive line sources are introduced and are shown to provide asymmetrical polar responses in the vertical plane. Such asymmetry is useful in many sound-reinforcement venues, and this is why so many contemporary loudspeaker line arrays are based on these configurations. The paper provides analytical models for both types and illustrates typical performance. Of particular note, progressive arrays produce a vertical polar response that is remarkably constant with frequency over a very wide bandwidth.

Third, line arrays of real loudspeakers are not perfectly continuous line sources, and this may introduce anomalies

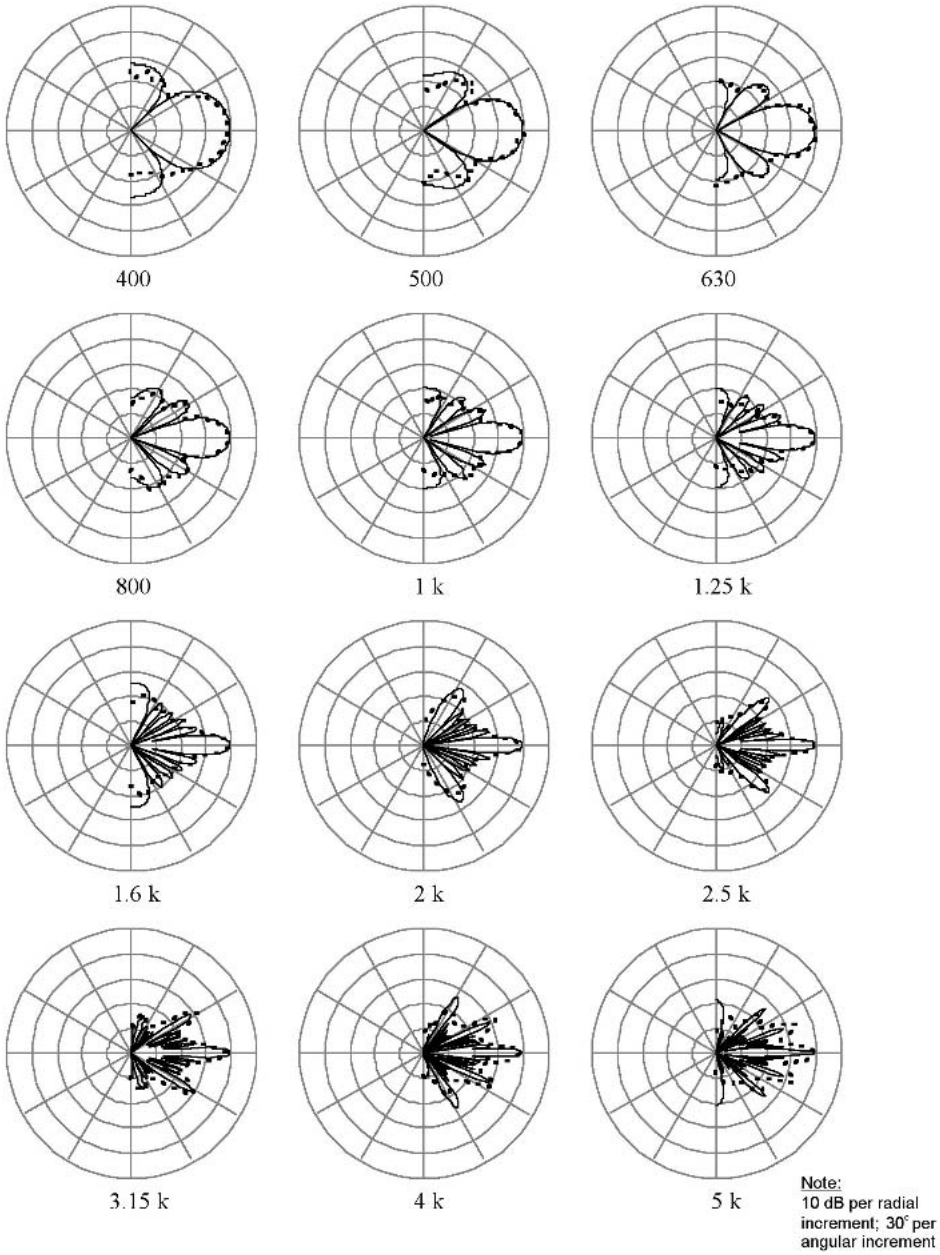

Fig. 43. Measured (· · ·) versus modeled (——) polar response curves of array in Fig. 41. Model based on a stack of arc sources with a sine wave input. Measured data are one-third-octave pink noise.

Fig. 44. Indoor ground-plane setup for vertical polar response measurements of eight-element curved array.

into their response. The paper provides a model that shows the effect of gaps in line sources that are introduced by the thickness of the loudspeaker enclosure construction material. The model shows that at low frequency, where the gap length is a small fraction of the wavelength, gaps have very little effect. At high frequency the sidelobe structure changes materially with the gap length. The lobes get wider and change position. As a practical matter, contemporary loudspeaker line array enclosures are usually designed to maximize the radiating percentage, often in excess of 90%. This minimizes the effects of gaps across the useful bandwidth.

Fourth, real loudspeaker elements may not produce perfectly flat wavefronts, so that a vertical stack of loudspeakers does not provide a perfectly straight-line source. The paper provides an analytical model to estimate the effect

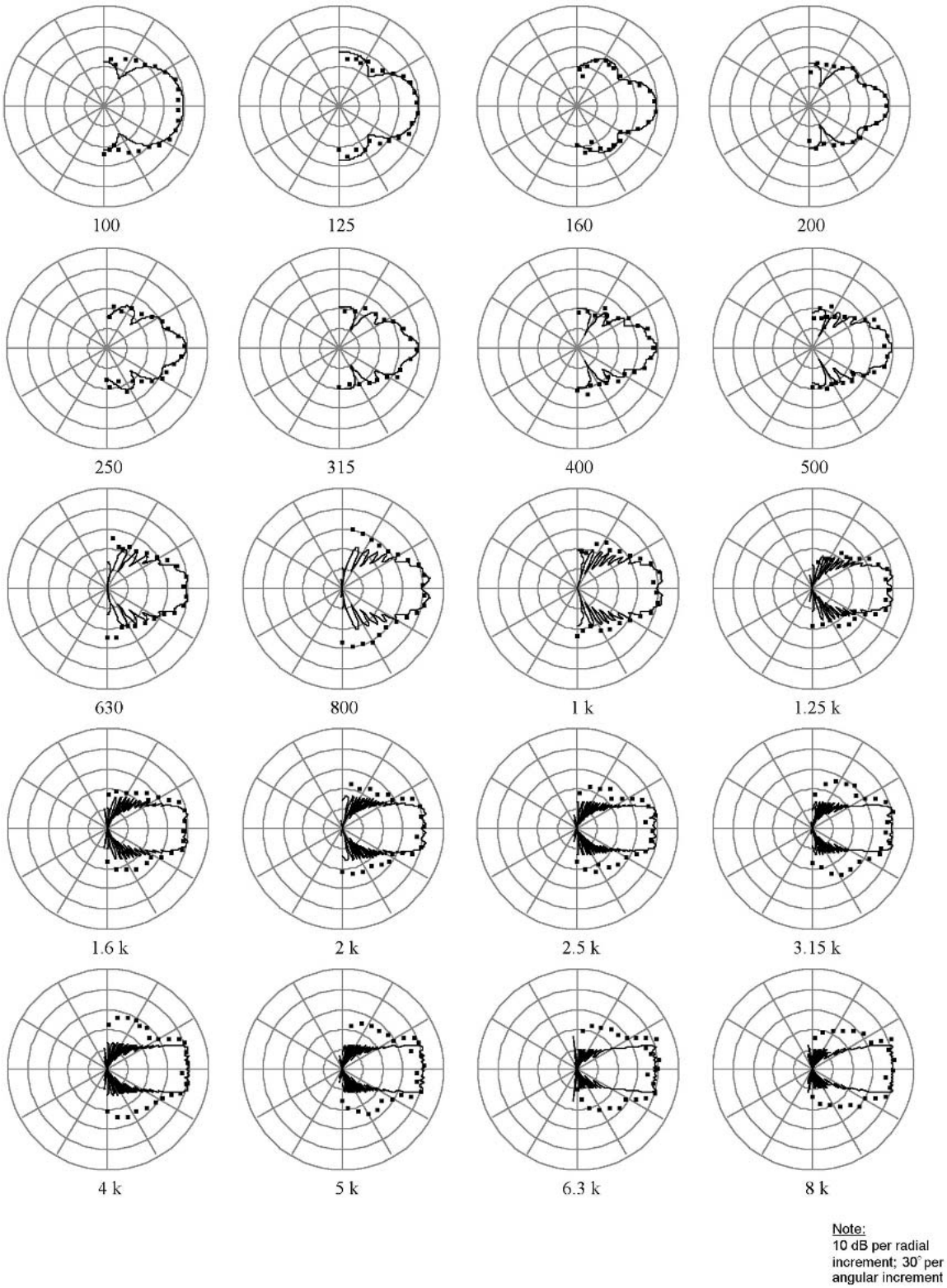

Fig. 45. Measured polar response data (· · ·) shown against predicted polar response of eight-element curved array.

of the curvature of the elemental sources of a line array. It shows that the effects are frequency dependent and negligible as long as the curvature is less than one-quarter wavelength.

Finally, measured polar response data of two different loudspeaker line arrays were compared to modeled results. In general the models produce very good estimates of actual performance despite the fact that loudspeaker nonlinearities, enclosure diffraction, and environmental effects among others are not accounted for. Robust results can be obtained for a wide variety of array types across an extended frequency range of interest.

ACKNOWLEDGMENT

The author would like to express his appreciation to his colleagues at JBL Professional, including Mark Gander, David Scheirman, Mark Engebretson, and Doug Button. They piqued his interest in line arrays, encouraged and supported this body of work, and were always fun to work with.

10 REFERENCES

[1] D. L. Klepper and D. W. Steele, "Constant Directional Characteristics from a Line Source Array," *Audio Eng. Soc.,* vol. 11, no. 3, p. 198 (1963).

[2] H. F. Olson, *Elements of Acoustical Engineering,* 1st ed. (Van Nostrand, New York, 1940), p. 25.

[3] I. Wolff and L. Malter, "Directional Radiation of Sound, *J. Acoust. Soc. Am.,* vol. 2, no. 2, p. 201 (1930).

[4] L. Beranek, *Acoustics,* 1st ed. (McGraw-Hill, New York, 1954).

[5] A. B. Wood, *A Textbook of Sound* (Bell and Sons, London, 1957).

[6] A. H. Davis, *Modern Acoustics,* 1st ed. (Macmillan, New York, 1934), p. 63.

[7] M. Rossi, *Acoustics and Electroacoustics* (Artech House, Norwood, MA, 1988).

[8] E. Skudrzyk, *The Foundations of Acoustics* (Springer, New York, 1971).

[9] S. P. Lipshitz and J. Vanderkooy, "The Acoustic Radiation of Line Sources of Finite Length," presented at the 81st Convention of the Audio Engineering Society, *J. Audio Eng. Soc.* (*Abstracts*), vol. 34, pp. 1032–1033 (1986 Dec.), preprint 2417.

[10] D. L. Smith, "Discrete-Element Line Arrays—Their Modeling and Optimization," *J. Audio Eng. Soc.,* vol. 45, pp. 948–964 (1997 Nov.).

[11] J. Eargle, *Handbook of Sound System Design* (ELAR Publ., Commack, NY, 1989).

[12] C. Heil, "Sound Fields Radiated by Multiple Sound Source Arrays," presented at the 92nd Convention of the Audio Engineering Society, *J. Audio Eng. Soc.* (*Abstracts*), vol. 40, p. 440 (1992 May), preprint 3269.

[13] M. Junger and D. Feit, *Sound, Structures, and Their Interactions* (MIT Press, Cambridge, MA, 1972).

[14] M. S. Ureda, "Line Arrays: Theory and Applications," presented at the 110th Convention of the Audio Engineering Society, *J. Audio Eng. Soc.* (*Abstracts*), vol. 49, p. 526 (2001 June), convention paper 5304.

[15] M. S. Ureda, "J and Spiral Line Arrays," presented at the 111th Convention of the Audio Engineering Society, *J. Audio Eng. Soc.* (*Abstracts*), vol. 49, p. 1233 (2001 Dec.), convention paper 5485.

[16] M. S. Urban, C. Heil, and P. Bauman, "Wavefront Sculpture Technology," *J. Audio Eng. Soc.* (*Engineering Reports*), vol. 51, pp. 912–932 (2003 Oct.).

[17] D. Button, "High-Frequency Components for High-Output Articulated Line Arrays," presented at the 113th Convention of the Audio Engineering Society, *J. Audio Eng. Soc.* (*Abstracts*), vol. 50, p. 957 (2002 Nov.), convention paper 5650.

[18] M. E. Engebretson, M. S. Ureda, and D. J. Button, "Directional Radiation Characteristics of Articulating Line Array Loudspeaker Systems," presented at the 111th Convention of the Audio Engineering Society, *J. Audio Eng. Soc.* (*Abstracts*), vol. 49, p. 1233 (2001 Dec.).

[19] J. E. Benson, "Theory and Applications of Electrically Tapered Electro-Acoustic Arrays," in *IREE Int. Electronics Conv. Digest* (1975 Aug.), pp. 587–589.

[20] L. Kinsler, A. Frey, A. Coppens, and J. Sanders, *Fundamentals of Acoustics,* 4th ed. (Wiley, New York, 1982).

[21] M. S. Ureda, "Wave Field Synthesis with Horn Arrays," presented at the 100th Convention of the Audio Engineering Society, *J. Audio Eng. Soc.* (*Abstracts*), vol. 44, p. 630 (1996 July/Aug.), preprint 4144.

THE AUTHOR

Mark Ureda received a B.S. degree in engineering from UCLA, an M.S. degree in acoustics from Penn State, and an M.B.A. from the UCLA Graduate School of Management.

Mr. Ureda joined the Altec Lansing Corporation in 1976 as an engineer in the acoustics research group. There he codeveloped the Mantaray constant directivity horns. In 1980 he was promoted to director of acoustics and led the development of several new lines of horns and loudspeakers. He left the company when it was sold in 1984 and began a career in aerospace. He returned to audio in 1990 as a consultant to Mark IV Audio, where he developed ArraySHOW, a software package that computes radiated sound fields of horn arrays. In 1999 he joined JBL Professional and developed the VerTec line array calculator. Audio is a hobby for him. He continues his aerospace career at Northrop Grumman, where he is the corporate vice president of Strategy and Technology. He is responsible for strategy development and mergers and acquisitions in the space and electronics segments.

Mr. Ureda has authored numerous technical papers on horns, directivity measurements, line sources, and loudspeaker/horn arrays.